Evaluating the "Rich-Get-Richer" Mechanism in Tropical Precipitation Change under Global Warming

CHIA CHOU

Research Center for Environmental Changes, Academia Sinica, and Department of Atmospheric Sciences, National Taiwan University, Taipei, Taiwan

J. DAVID NEELIN

Department of Atmospheric and Oceanic Sciences and Institute of Geophysics and Planetary Physics, University of California, Los Angeles, Los Angeles, California

CHAO-AN CHEN

Research Center for Environmental Changes, Academia Sinica, Taipei, Taiwan

JIEN-YI TU

Department of Atmospheric Sciences, Chinese Culture University, Yang-Ming Shan, Taipei, Taiwan

(Manuscript received 6 February 2008, in final form 24 October 2008)

ABSTRACT

Examining tropical regional precipitation anomalies under global warming in 10 coupled global climate models, several mechanisms are consistently found. The tendency of rainfall to increase in convergence zones with large climatological precipitation and to decrease in subsidence regions—the rich-get-richer mechanism—has previously been examined in different approximations by Chou and Neelin, and Held and Soden. The effect of increased moisture transported by the mean circulation (the "direct moisture effect" or "thermodynamic component" in respective terminology) is relatively robust, while dynamic feedback is poorly understood and differs among models. The argument outlined states that the thermodynamic component should be a good approximation for large-scale averages; this is confirmed for averages across convection zones and descent regions, respectively. Within the convergence zones, however, dynamic feedback can substantially increase or decrease precipitation anomalies. Regions of negative precipitation anomalies within the convergence zones are associated with local weakening of ascent, and some of these exhibit horizontal dry advection associated with the "upped-ante" mechanism. Regions of increased ascent have strong positive precipitation anomalies enhanced by moisture convergence. This dynamic feedback is consistent with reduced gross moist stability due to increased moisture not being entirely compensated by effects of tropospheric warming and a vertical extent of convection. Regions of reduced ascent with positive precipitation anomalies are on average associated with changes in the vertical structure of vertical velocity, which extends to higher levels. This yields an increase in the gross moist stability that opposes ascent. The reductions in ascent associated with gross moist stability and upped-ante effects, respectively, combine to yield reduced ascent averaged across the convergence zones. Over climatological subsidence regions, positive precipitation anomalies can be associated with a convergence zone shift induced locally by anomalous heat flux from the ocean. Negative precipitation anomalies have a contribution from the thermodynamic component but can be enhanced or reduced by changes in the vertical velocity. Regions of enhanced subsidence are associated with an increased outgoing longwave radiation or horizontal cold convection. Reductions of subsidence are associated with changes of the vertical profile of vertical velocity, increasing gross moist stability.

Corresponding author address: Chia Chou, Research Center for Environmental Changes, Academia Sinica, P.O. Box 1–48, Taipei 11529, Taiwan.
E-mail: chiachou@rcec.sinica.edu.tw

DOI: 10.1175/2008JCLI2471.1

1. Introduction

Predicting future temperature changes under global warming is a challenging task, but predicting future precipitation changes may be even more difficult. The agreement among climate model simulations on the spatial distribution of time mean precipitation changes tends to be very poor, especially at a regional scale (e.g., Cubasch et al. 2001; Allen and Ingram 2002; Stott and Kettleborough 2002; Neelin et al. 2006; Meehl et al. 2007). This paper aims to contribute moisture and energy budget analysis of balances and mechanisms contributing to such precipitation changes in the tropics.

Before addressing the specific questions associated with this, we note that there are a number of aspects of precipitation change under global warming that are better documented. A number of model studies indicate that increased precipitation intensity and decreased precipitation frequency will most likely occur associated with the warming (recently, Wilby and Wigley 2002; Trenberth et al. 2003; Kharin and Zwiers 2005; Meehl et al. 2005; Barnett et al. 2006; Sun et al. 2007). Evidence for such changes has also been sought in observations, as reviewed in Trenberth et al. (2007). Despite imperfect simulation of precipitation distributions in climate models (e.g., Dai and Trenberth 2004; Dai 2006; Wilcox and Donner 2007), these effects are thought to be robust because of a simple underlying argument. Moisture content available for extreme events tends to increase at a rate roughly governed by the Clausius–Clapeyron equation, while the energy available to drive convection (for averages over sufficiently large scales that transports are negligible) increases less quickly (e.g., Allen and Ingram 2002; Meehl et al. 2007).

Increased precipitation at high latitudes and decreased precipitation in the subtropics is a common feature among climate models, while in the annual average the deep tropics tend to have a precipitation increase (Meehl et al. 2007). Examining precipitation change averaged over latitudinal bands, Zhang et al. (2007) argued for detectable human impacts on precipitation, with larger amplitudes in observations than in model simulations. Even at regional scales, a few areas exhibit precipitation change that is consistent among model simulations (Christensen et al. 2007). For instance, relatively consistent projections are noted for twenty-first-century decreasing trends of precipitation in southern Europe (Rowell and Jones 2006), southwestern North America (Milly et al. 2005; Seager et al. 2007), parts of Southeast Asian dry seasons (Li et al. 2007), and the Caribbean–Central America region in summer (Neelin et al. 2006) where an observed trend is also noted.

In the tropics, at large scales on the annual average, Held and Soden (2006, hereafter HS06) sought robust features among climate models and found a weakening of the tropical circulation, which tends to compensate the effect of the increased atmospheric moisture on tropical precipitation in convergence zones. Chou et al. (2007) studied hemispherical averages of tropical precipitation and found a widening of the seasonal precipitation range between wet and dry seasons to be common among models. For large spatial averages, Neelin et al. (2006) used a measure of the amplitude for the increase and decrease of regional precipitation of each model and found these amplitudes to agree relatively well among climate models even if the locations of the strong changes differed.

Despite these areas where some agreement among climate models and observations can be found, very substantial differences in the geographic distribution of precipitation changes are typical not only at the regional scale but even for relatively large spatial averages (e.g., Allan and Soden 2007, 2008; Chou et al. 2007; Trenberth and Dai 2007; Trenberth et al. 2007; Wentz et al. 2007; Zhang et al. 2007) and in the tropical examples to be examined here.

Among mechanisms for regional change of mean tropical precipitation, Chou and Neelin (2004, hereafter CN04) and HS06 proposed closely related approaches, both of which are built on arguments by Manabe and coworkers (Manabe and Wetherald 1975; Knutson and Manabe 1995; Wetherald and Manabe 2002). The term ''rich-get-richer mechanism'' is appropriate for both variants, since the essence of the mechanism is to tend to enhance precipitation in regions that already have strong moisture convergence and precipitation. We will attempt to clarify the relationship between the two studies as we examine the mechanism in more detail. At its most basic, in a warmer climate, the atmospheric moisture tends to increase, governed by the Clausius–Clapeyron expansion with relative humidity that tends to change less strongly (often approximated as constant). If one ignores changes in the flow, regions with climatological convergence/divergence will tend to have an increased moisture convergence/divergence, which tends to yield precipitation increases in tropical convergence zones and decreases in descent regions. However, additional factors immediately enter. CN04 noted that moisture increases at low levels tend to reduce the gross moist stability (Yu et al. 1998) unless there is a compensating increase in the dry stability component. Reduced gross moist stability would yield an enhanced ascent in ascending regions, providing a dynamic feedback that can potentially increase the precipitation. However, increased dry static energy due to warming or increased depth of convection can oppose this effect. The lack of theory for changes in the gross moist stability

yields uncertainties in the dynamic convergence feedback, which locally can be large (Chou et al. 2006).

The moisture increase is also not uniform—moisture within the convergence zones tends to increase through a deeper layer because of the convection, creating horizontal gradients of the moisture anomalies. This yields another mechanism that operates in certain regions of the convective margin (Neelin et al. 2003; CN04), the "upped-ante" mechanism. Dry advection associated with inflow from the less-moistened subsidence regions into the convergence zones tends to suppress convection in the convective margin regions. The upped-ante mechanism is thus one means by which the margin of the convergence zone can be shifted inward (noting that because the margin has a finite width, the anomalies tend to be spread out over a region larger than the shift in a particular contour of precipitation or moisture convergence). Precipitation in the convective margins is reduced and the convergence feedback weakens the ascent, which weakens the tropical circulation. We note that the horizontal gradient of the moisture anomalies can be smoothed out slightly by horizontal transport, which tends to yield a more constant relative humidity (Soden et al. 2005).

CN04 emphasizes dynamic feedbacks, such as the convergence feedback, enhancing thermodynamic effects because of the increase in moisture and moisture gradients. HS06 emphasizes the robust aspects of the thermodynamic effects, especially in the annual average, ensemble average, and zonal average. Under the hypothesis that many of the regional discrepancies among climate models are associated with dynamic feedbacks, we use moist static energy (MSE) diagnostics informed by the hypothesized mechanisms of CN04 to examine processes affecting regional tropical precipitation change. We analyze 10 coupled general circulation model (CGCM) simulations in order to seek consistent budgetary balances associated with mechanisms that induce regional change of mean tropical precipitation within and outside the convergence zones. Changes in rainfall distribution characteristics, though important, are not discussed here. In section 2, we briefly describe the data and the moisture and MSE budgets, clarifying the relationship between CN04 and HS06 in terms of these budgets. For reasons outlined below, the analysis carried out separately for tropical convergence zones and subsidence regions, respectively, in sections 3 and 4. The discussion and conclusions are in section 5.

2. Data and formula

a. Data

Data are from the climate model simulations in the archive supported by the Program for Climate Model Diagnosis and Intercomparison for the Fourth Assessment Report (AR4) of the Intergovernmental Panel on Climate Change (IPCC). The A2 scenario for anthropogenic emissions is used. Since the A2 scenario is at the higher end of the IPCC emission scenario, the warming is larger than other scenarios, such as the A1B scenario, but spatial patterns and mechanisms are expected to be similar no matter what scenario is used. One realization from each of the 10 models is used. The models that we chose are based on the data availability. The NCAR PCM1 and GISS-ER models Table 1 do not have all components of surface heat fluxes, so the corresponding net energy into the atmospheric column F^{net} is calculated only in 8 models; other variables are calculated in all 10 models. We define the period of 1961–90 as current climate and use the period of 2070–99 for future climate. All anomalies shown in this study are differences between these two periods. The climate model simulations used here are briefly described in Table 1 and a detailed description can be found online (http://www-pcmdi.llnl.gov/ipcc/model_documentation/ipcc_model_documentation.php).

b. Moisture and moist static energy budgets

To understand mechanisms that induce tropical precipitation anomalies, the vertically integrated moisture budget,

$$P' = -\langle \bar{\omega}\partial_p q' \rangle - \langle \omega' \partial_p \bar{q} \rangle - \langle \mathbf{v} \cdot \nabla q \rangle' + E' + \text{residual\_}q, \tag{1}$$

is diagnosed first, where $(\bar{})$ denotes climatology in 1961–90, which is defined as current climate. Here $()'$ represents the departure from the current climate. The precipitation P is in energy units (W m^{-2}) which, divided by 28, becomes mm day^{-1}. The E is evaporation, ω is pressure velocity, $\mathbf{v}$ is horizontal velocity, and the specific humidity q is in energy units by absorbing the latent heat per unit mass, L. Vertical integral $\langle\ \rangle$ denotes a mass integration through the troposphere with p_T as the depth of the troposphere:

$$\langle X \rangle = g^{-1} \int_{p_s}^{p_s - p_T} X dp, \tag{2}$$

where g is gravity and p_s is surface pressure. Because tropical convection affects layers above the convection heating (Holloway and Neelin 2007), the vertical integral from 1000 to 30 hPa is used in this study, much higher than the tropopause. In (1), precipitation anomalies are roughly balanced by anomalous vertical moisture transport associated with mean flow ($\bar{\omega}$) and anomalous flow

TABLE 1. A list of the 10 coupled atmosphere–ocean climate model simulations in the A2 scenario from the Program for Climate Model Diagnosis and Intercomparison for the AR4 of the IPCC.

Model	Description
CA CCCMA3.1 T47	Canada, Canadian Centre for Climate Modeling and Analysis (CCCMA), CGCM3.1 Model, T47
FR CNRM CM3	France, Centre National de Research Meteorologiques (CNRM), CM3
JP MRI2.3	Japan, Meteorological Research Institute (MRI) Coupled General Circulation Model, version 2.3.2a (CM2.3.2a)
GFDL CCM2.0	National Oceanic and Atmospheric Administration (NOAA) Geophysical Fluid Dynamics Laboratory (GFDL), CM2.0
GISS-ER	National Aeronautics and Space Administration (NASA) Goddard Institute for Space Studies (GISS;Model E20/Russell)
NCAR CCSM3	NCAR Community Climate System Model (CCSM), CM3
NCAR PCM1	NCAR Parallel Climate Model (PCM; version 1)
MPI ECHAM5	Germany, Max Planck Institute for Meteorology (MPI), ECHAM5
UKMO HadCM3	United Kingdom, third climate configuration of the Met Office Unified Model
UKMO HadGEM1	United Kingdom, Hadley Centre Global Environmental Model version 1

(ω'), anomalous horizontal moisture transport, and evaporation anomalies. The residual_q term includes transient and nonlinear terms, such as $-\langle\omega'\partial_p q'\rangle$.

The second term on the right of (1) is a dynamical feedback associated with anomalous circulation ω'. Insight into the terms that balance ω' can be obtained from the vertically integrated MSE budget, which can be written as

$$\langle\omega'\partial_p\bar{h}\rangle = -\langle\bar{\omega}\partial_p h'\rangle - \langle\mathbf{v}\cdot\nabla(q+T)\rangle' + F^{\text{net}'} + \text{residual\_}h, \tag{3}$$

where T is atmospheric temperature in energy units, that is, absorbing the heat capacity at constant pressure C_p. The MSE is $h = q + s$, and the dry static energy is $s = T + \phi$, with ϕ being the geopotential. The net energy flux into the atmospheric column is

$$F^{\text{net}} = F_t - F_s. \tag{4}$$

The net heat flux at the top of the atmosphere (TOA) is

$$F_t = S_t^{\downarrow} - S_t^{\uparrow} - R_t^{\uparrow}, \tag{5}$$

and the net heat flux at the surface is

$$F_s = S_s^{\downarrow} - S_s^{\uparrow} + R_s^{\downarrow} - R_s^{\uparrow} - E - H. \tag{6}$$

Subscripts s and t on the solar ($S^{\downarrow}$ and $S^{\uparrow}$) and longwave ($R^{\uparrow}$ and $R^{\downarrow}$) radiative terms denote surface and model top, and H is sensible heat flux. Positive F_t and F_s indicate downward heat fluxes. Besides transients and the nonlinear term $\langle\omega'\partial_p h'\rangle$, such as in the residual_q term, the residual_h term also includes contributions from dry static energy transport from upper levels in the atmosphere, because we evaluate the transports over a tropospheric and lower stratospheric layer, specifically for pressures greater than 30 hPa. These contributions tend to be small when convection is the dominant process affecting the vertical distribution of tropospheric MSE, provided that the lower stratosphere is included—we find that vertical motions associated with convection often have a nontrivial contribution just above the top of convection, consistent with Holloway and Neelin (2007). In (3), the term associated with ω', that is, $\langle\omega'\partial_p\bar{h}\rangle$, is roughly balanced by anomalous vertical MSE transport associated with mean flow, horizontal MSE transport anomalies, and $F^{\text{net}'}$.

c. *Mechanisms in approximate moist static energy budgets*

We now discuss approximations to the above budgets that can inform our understanding of the mechanisms (these approximations are not used in the actual analysis, only for discussion). Based on the quasi-equilibrium assumption for deep convection discussed in CN04, defining a typical vertical profile of vertical motion $\Omega(p)$ of deep convection, the vertically integrated vertical moisture transport $-\langle\omega\partial_p q\rangle$, can be rewritten as

$$-\langle\omega\partial_p q\rangle \approx M_q\nabla\cdot\mathbf{v}_1, \tag{7}$$

where $\nabla\cdot\mathbf{v}_1$ is divergence induced by baroclinic winds. The gross moisture stratification (Neelin and Yu 1994; Yu et al. 1998) is

$$M_q = \langle\Omega\partial_p q\rangle. \tag{8}$$

Positive $\nabla\cdot\mathbf{v}_1$ is indicates low-level convergence and upper-level divergence in baroclinic flow. Following a similar derivation, $\langle\omega\partial_p h\rangle \approx M\nabla\cdot\mathbf{v}_1$ and $\langle\omega\partial_p s\rangle \approx M_s\nabla\cdot\mathbf{v}_1$ with $M = \langle-\Omega\partial_p h\rangle$ and $M_s = \langle-\Omega\partial_p s\rangle$. Note that $M = M_s - M_q$. In this notation, (1) simplifies to

$$P' = M_q'\nabla\cdot\bar{\mathbf{v}}_1 + \bar{M}_q\nabla\cdot\mathbf{v}_1' - \langle\mathbf{v}\cdot\nabla_q\rangle' + E', \tag{9}$$

while (3) can be rewritten to obtain anomalous vertical motion:

$$\nabla \cdot \mathbf{v}_1' \approx \bar{M}^{-1}[-M'\nabla \cdot \bar{\mathbf{v}}_1 + F^{\text{net}'} - <\mathbf{v} \cdot \nabla(q+T)>']. \tag{10}$$

The anomalies of the divergent circulation $\nabla \cdot \mathbf{v}_1'$, and corresponding vertical motion, have substantial precipitation anomalies associated with them. In (10), the variations of the tropical convection and circulation are determined by the variation of gross moist stability M, the net energy into the atmosphere, and the horizontal MSE advection.

In convective centers, omitting the horizontal moisture and temperature gradient terms, evaporation anomalies, and $F^{\text{net}'}$, the precipitation anomalies can be estimated (CN04) by

$$P' \approx \nabla \cdot \bar{\mathbf{v}}_1 \left[\frac{\bar{M}_q}{\bar{M}}(-M') + M_q'\right]. \tag{11}$$

Equation (11) can be used to represent the rich-get-richer mechanism: terms in M' and M_q' are multiplied by the climatological convergence, so if M' is negative and M_q' is positive under warming, they yield precipitation increases in climatological convergence zones and decreases in descent regions. Increases in moisture yield positive M_q'; since $M' = M_s' - M_q'$, the M' term will have the opposite sign *unless* M_s' increases overcompensate. The effect associated with $M_q'\nabla \cdot \bar{\mathbf{v}}_1$ is the "direct moisture effect" (CN04 terminology) or the "thermodynamic" component of the local hydrological response (HS06 terminology). The effect associated with M' affects tropical precipitation via $\nabla \cdot \bar{\mathbf{v}}_1$, a dynamic feedback sometimes referred to as the convergence feedback. In other words, tropical precipitation is affected directly by moisture change, that is, M_q', and by a dynamic feedback, that is, the term associated with M'. The HS06 approximation to CN04 is equivalent to neglecting the M' term. More insight can be drawn by noting that, if one neglects $\nabla \cdot \bar{\mathbf{v}}_1$ as in the HS06 discussion of the "thermodynamic" component, the energy budget (10) is not needed and the HS06 approximation to (11) is obtained directly:

$$P' \approx M_q'\nabla \cdot \bar{\mathbf{v}}_1, \tag{12}$$

which tends to follow the Clausius–Clapeyron relation. From this we can anticipate that any average that tends to reduce the more localized $\nabla \cdot \bar{\mathbf{v}}_1$ contribution will make (12) a better approximation. Large spatial averages will reduce $\nabla \cdot \mathbf{v}_1'$, but so will ensemble averages if locations disagree as the regions of positive and negative $\nabla \cdot \mathbf{v}_1'$ partially cancel.

In convective margin regions, if $\nabla \cdot \mathbf{v}_1'$ is affected mainly by $-\langle \mathbf{v} \cdot \nabla q \rangle'$, the precipitation anomalies can be estimated by

$$P' \approx \left(1 + \frac{\bar{M}_q}{\bar{M}}\right)(-\langle \mathbf{v} \cdot \nabla q \rangle'). \tag{13}$$

According to (13), tropical precipitation is affected directly by horizontal moisture advection and by a dynamic feedback ($\frac{\bar{M}_q}{\bar{M}}$) associated with horizontal moisture convergence. The convergence feedback tends to be larger than the direct effect associated with moisture advection since $\frac{\bar{M}_q}{\bar{M}}$ is greater than 1. The dry advection is responsible for the overall effect (as may be seen since it multiplies both terms), consistent with the upped-ante mechanism (CN04). This reduction of low-level convergence could partly result in a weakening of the Walker circulation (Vecchi et al. 2006). However, just how big this area is will be examined later and remains to be seen.

d. Classification of subregions in the tropics

To have a point of reference, we choose current climatology to divide the tropics into dynamically motivated regions. One can also use measures that change with the climate, for example, HS06 and Vecchi and Soden (2007), and we have obtained similar results with a measure using moisture change rather than climatology. The choice here aids examination of the spatial distribution of tropical precipitation changes relatively to its own climatology, which varies among climate models. Here we first define climatologically ascending and descending areas. While one might use convective mass flux or vertical velocity at midtroposphere, we use a directly relevant term, the vertical moisture transport associated with mean circulation $-\langle \bar{\omega}\partial_p \bar{q} \rangle$, to define ascending and descending areas. An area with $-\langle \bar{\omega}\partial_p \bar{q} \rangle > 0$ is defined as an ascending region, and an area with $-\langle \bar{\omega}\partial_p \bar{q} \rangle < 0$ is defined as a descending region, so the curve with $-\langle \bar{\omega}\partial_p \bar{q} \rangle = 0$ is drawn in figures as the boundary of the ascending and descending areas.

Figure 1 shows the boreal winter [December–January (DJF)] and summer [June–August (JJA)] precipitation differences between future (2070–99) and current (1961–90) climates for 10 CGCM simulations in the A2 scenario. The boundary of the convergence zones defined by $-\langle \bar{\omega}\partial_p \bar{q} \rangle = 0$ (dark solid curves) is similar to the 4 mm day^{-1} contour of climatological precipitation in 1961–90 (e.g., light dashed curves in Fig. 1), so the convergence zones defined here represent most of the regions with mean precipitation greater than 4 mm day^{-1}. This also provides justification for the previous use of 4 mm day^{-1} to estimate the boundary of

the convergence zones (Chou et al. 2006). The $-\langle\bar{\omega}\partial_p\bar{q}\rangle = 0$ contour is also similar to the zero 500-hPa vertical velocity contour (not shown), that is, $\bar{\omega}_{500} = 0$, which is commonly used to define convergence zones.

Figure 1 indicates that most large positive precipitation anomalies are over either convective regions or their margins, while large negative precipitation anomalies tend to be over margins of convective regions, often with the largest anomalies occurring inside the zero moisture convergence line. Positive anomalies within the convection zones are potentially consistent with CN04 and HS06, while positive anomalies in certain margins, for instance in the equatorial cold tongue, may be associated with ocean feedback and shifts of atmospheric circulation (Chou et al. 2006; Chung and Ramanathan 2007; Emori and Brown 2005; Lu et al. 2007; Seidel et al. 2007). Negative anomalies along convective margins with the inflow from dry regions have been hypothesized to be associated with the upped-ante mechanism. In Fig. 2 it may be seen that shifts of the convergence zone boundary (as measured by zero mean flow moisture convergence) are in a direction consistent with the anomalies along the boundary. However, the shift of this moisture convergence boundary is typically smaller than the area over which precipitation anomalies occur, because the margins are not sharp. Convective margin effects are thus often seen, for instance, as reduction of precipitation near the convective margin, but still with the same sign of the moisture convergence as in climatology. Note that these effects can still potentially be described as a shift or alteration of the convective margin—it is simply that most of the anomaly remains within a region for which the sign of the moisture convergence is not changed. All 10 models show similar effects. One convenient consequence of this is that for some purposes one can define averaging regions based on moisture convergence in current climate and still capture most of the near-margin anomalies. Examining Fig. 1 further, both positive and negative precipitation anomalies are found over ascending regions for all 10 model simulations. This is also the case over descending regions.

To present the relative importance of budget terms for a tractable number of regions, we thus divide the tropics into four main analysis regions: positive and negative precipitation anomalies over climatological ascending and descending regions. Finally, each region is further divided by different signs of $-\langle\omega'\partial_p\bar{q}\rangle$, which is associated with anomalous vertical velocity. The subregions in the tropics are summarized in Fig. 2 and Table 2. In Fig. 2, the ascending and descending regions are divided by black thick curves. Within the convergence zones, the area I with negative precipitation anomalies (subset I) is in red, while the area II with positive precipitation (subset II) is blue, which is further divided into two subregions: the area IIa with anomalous ascent is in dark blue and the area IIb with anomalous descent is in light blue. Outside the convergence zones, the area III with positive precipitation anomalies (subset III) is in blue, while the area IV with negative precipitation anomalies (subset IV) is in red, which is also divided into two subregions: the area IVa with anomalous descent is in dark red and the area IVb with anomalous ascent is in light red. We note that the regions are dynamically connected, the division being simply a means of condensing information on the relative importance of budget terms. Stratifying by measures of ascent/descent is common (e.g., Bony et al. 2006), and the further subdivision by the sign of precipitation anomalies is of interest because the simplest expectation (HS06; Meehl et al. 2007) would have been for increases within convergence zones and decreases in subsidence regions.

3. Precipitation changes over convective regions

a. Negative precipitation anomalies within ascending regions

Figure 1 shows that stronger negative precipitation anomalies are often found over the convective margins within the convergence zone. To understand the mechanisms that induce those negative precipitation anomalies, we first analyze vertically integrated moisture budgets averaged over the ascending regions with negative precipitation anomalies (area I). For most models, the spatially averaged precipitation change is less than -0.4 mm day^{-1} K^{-1} (Table 3). Only UKMO HadCM3 and UKMO HadGEM1 have a greater amplitude of precipitation change, decreasing more than 0.4 mm day^{-1} K^{-1}. Figure 3 shows that the first term on the right of (1), $-\langle\bar{\omega}\partial_p q'\rangle$, is positive since $\bar{\omega}$ is negative (upward motion) and the moisture changes usually concentrate in the lower troposphere. In other words, the vertical moisture transport associated with mean circulation, the direct moisture effect (CN04 terminology) or the thermodynamic component (HS06 terminology), tends to enhance tropical precipitation, which opposes the negative precipitation anomalies. On the other hand, the vertical moisture transport associated with anomalous vertical motion, $-\langle\omega'\partial_p\bar{q}\rangle$, is significantly less than zero. In fact, the magnitude of $-\langle\omega'\partial_p\bar{q}\rangle$ is greater than $-\langle\bar{\omega}\partial_p q'\rangle$, so the net effect associated with vertical moisture transport is negative, which is consistent with the negative precipitation anomalies (Fig. 3). Negative $-\langle\omega'\partial_p\bar{q}\rangle$ implies downward anomalous motion. Since most negative $-\langle\omega'\partial_p\bar{q}\rangle$ areas are located at convective

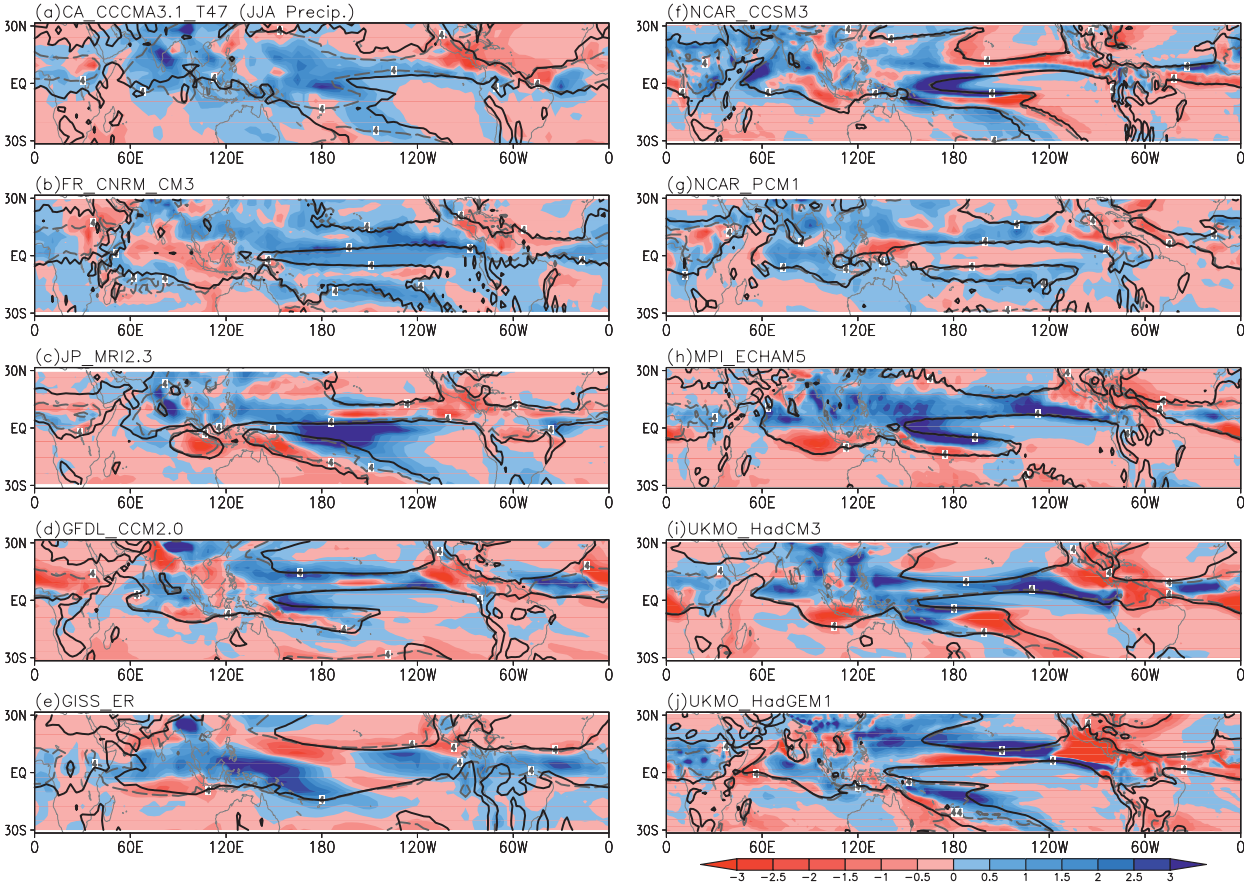

FIG. 1. Precipitation differences (mm day^{-1}) of 10 CGCM simulations (see Table 1) for the 2070–99 averages minus the 1961–90 climatology in the scenario A2 in (a)–(j) JJA and (k)–(t) DJF. The thick dark solid line is the $-\langle\bar{\omega}\partial_p\bar{q}\rangle = 0$ contour and the thick light dashed line is the 4 mm day^{-1} contour of the precipitation climatology in 1961–90.

margins, it is possible that the downward anomalous motion is associated with a shift of convergence zones. Figure 4 shows that mean vertical velocity in the period of 2070–99 is still upward even though the anomalous vertical motion is downward. While it is important that these regions occur in the margin of convection zone, the main areas of the anomalies are associated with reduction of convergence, as opposed to a change in sign (see Fig. 2). Overall, negative $-\langle\omega'\partial_p\bar{q}\rangle$ implies reduced upward motion over these areas, so the associated convection is weakened. The horizontal moisture advection $-(\mathbf{v}\cdot\nabla q)'$ is negative, while the evaporation anomaly E' is positive (Fig. 3). The magnitude of both terms is relatively smaller than those of the vertical moisture transport terms. The residual_q term in the moisture budget (1) is negative (not shown), as is $-(\mathbf{v}\cdot\nabla q)'$. The residual_$q$ term is contributed to mostly by the nonlinear component of $-\langle\omega'\partial_p q'\rangle$ since the magnitude of ω' can be comparable to $\bar{\omega}$ over the convective margins, that is, a shift of convective margins. Overall, the magnitude of $-\langle\omega'\partial_p\bar{q}\rangle$ is the greatest, so the negative precipitation anomalies are mainly caused by the dynamic feedback via $-\langle\omega'\partial_p\bar{q}\rangle$, which implies the reduction of tropical convection and the corresponding circulation.

We further examine the spatial distribution of $-\langle\omega'\partial_p\bar{q}\rangle$ over the area I (Fig. 5). For brevity, only the NCAR CCSM3 results are shown here and in the rest of figures. The results that we emphasize are generally similar among most of the models, although details can vary at the regional level. Figure 5 clearly shows that most parts of the area I are associated with negative $-\langle\omega'\partial_p\bar{q}\rangle$. Positive $-\langle\omega'\partial_p\bar{q}\rangle$ is found only over a small portion of these ascending regions, such as Africa. In other words, in order to have negative precipitation anomalies over the convergence zones, the associated ascending motion must be reduced. This weakening of the ascending motion, which may be associated with the weakening of the Walker circulation (Vecchi et al. 2006), is consistently found among the 10 CGCM simulations used in this study. The question then becomes what causes the weakened ascending motion? We also

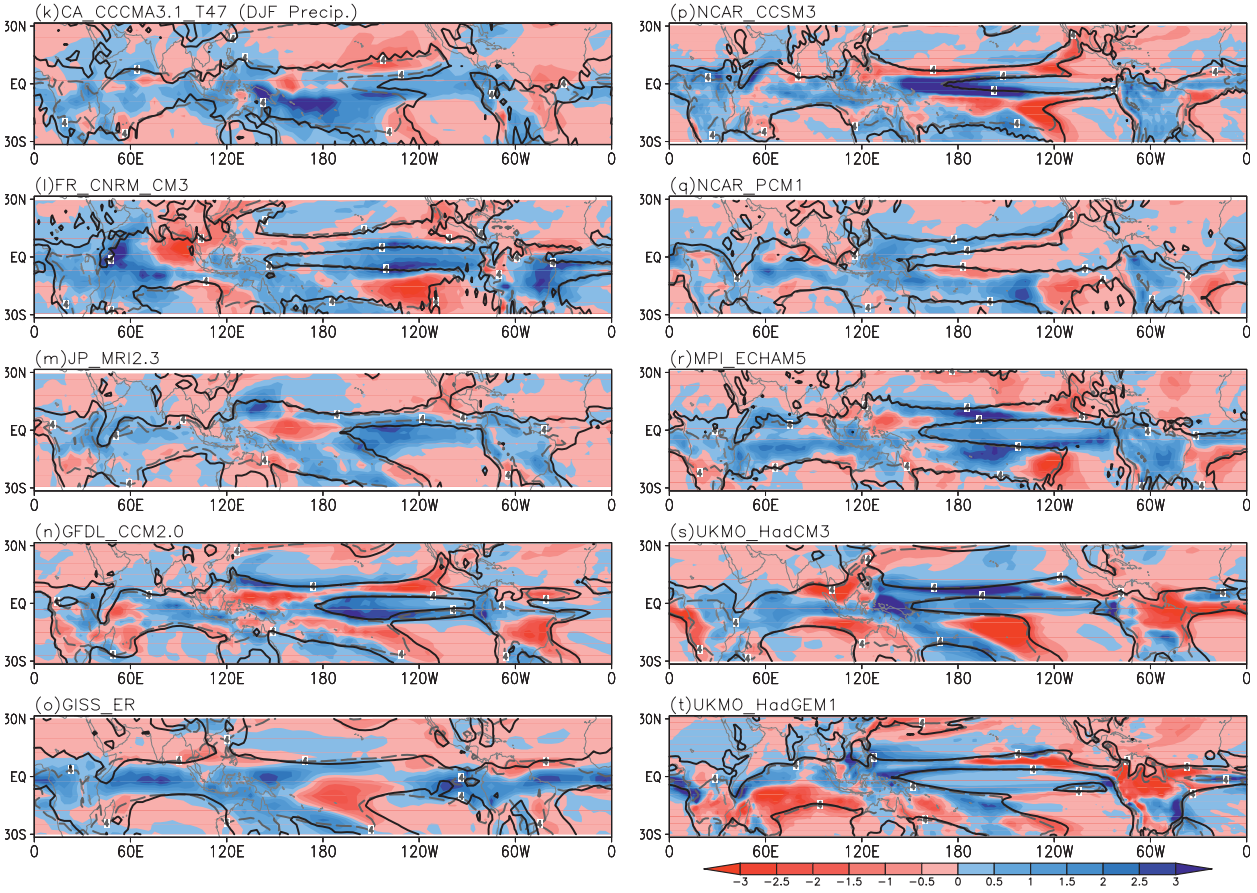

FIG. 1. (*Continued*)

notice that most negative $-\langle\omega'\partial_p\bar{q}\rangle$ are near the convective boundary, that is, the convective margins (thick solid curves). Such changes, which might be described as shifts in the convective margin, could be associated with the upped-ante mechanism discussed in CN04; or $-\langle\omega'\partial_p\bar{q}\rangle$ might be controlled by more complicated processes, since the CGCMs used in this study are much more complicated than the intermediate climate model in CN04.

To understand the vertical moisture transport associated with anomalous vertical motion and the weakening of the ascending motion over the area I in more comprehensive climate models, the vertically integrated MSE budget is analyzed (right-hand side of Fig. 3) to estimate the change of vertical motion, which is dominated by convective processes in the tropics. The term $\langle\omega'\partial_p\bar{h}\rangle$, which is on the left of (3), is negative since the amplitude of positive $-\langle\omega'\partial_p\bar{s}\rangle$ is slightly greater than negative $-\langle\omega'\partial_p\bar{q}\rangle$. Figure 3 shows $-\langle\omega'\partial_p\bar{h}\rangle$, instead of $\langle\omega'\partial_p\bar{h}\rangle$ shown in (3), to be consistent with the moisture budget shown in the same figure. Positive $-\langle\omega'\partial_p\bar{h}\rangle$ indicates downward anomalous motion, which is induced by effects shown on the rhs of (3). On the right of (3), $-\langle\bar{\omega}\partial_p h'\rangle$ is positive since the amplitude of positive $-\langle\bar{\omega}\partial_p q'\rangle$ is slightly greater than negative $-\langle\bar{\omega}\partial_p s'\rangle$. Here $-\langle\bar{\omega}\partial_p h'\rangle \approx -M'\nabla\cdot\bar{\mathbf{v}}_1$, which is associated with the convergence feedback in the rich-get-richer mechanism (CN04). Thus, the rich-get-richer mechanism here tends to induce upward anomalous motion and then enhances precipitation over the area I, which opposes the negative precipitation anomalies found in these areas. Both $-(\mathbf{v}\cdot\nabla q)'$ and $-(\mathbf{v}\cdot\nabla T)'$ are negative, but $-(\mathbf{v}\cdot\nabla q)'$ is larger than $-(\mathbf{v}\cdot\nabla T)'$. The effect associated with $-(\mathbf{v}\cdot\nabla q)'$ is the upped-ante mechanism (CN04). The $F^{\text{net}'}$ in a spatial average is relatively small, and so is the residual_h term (not shown). Overall for the spatial averages, the upped-ante mechanism and the similar effect of $-\langle\mathbf{v}\cdot\nabla T\rangle'$ are responsible for weakening the ascending motion over the area I.

When examining the spatial pattern of the terms on the right of (3), $-\langle\mathbf{v}\cdot\nabla q\rangle'$ dominates more than half of the area I, while $F^{\text{net}'}$ dominates around 20% of these areas (not shown). The residual_h term also contributes to the downward anomalous motion. The residual_h

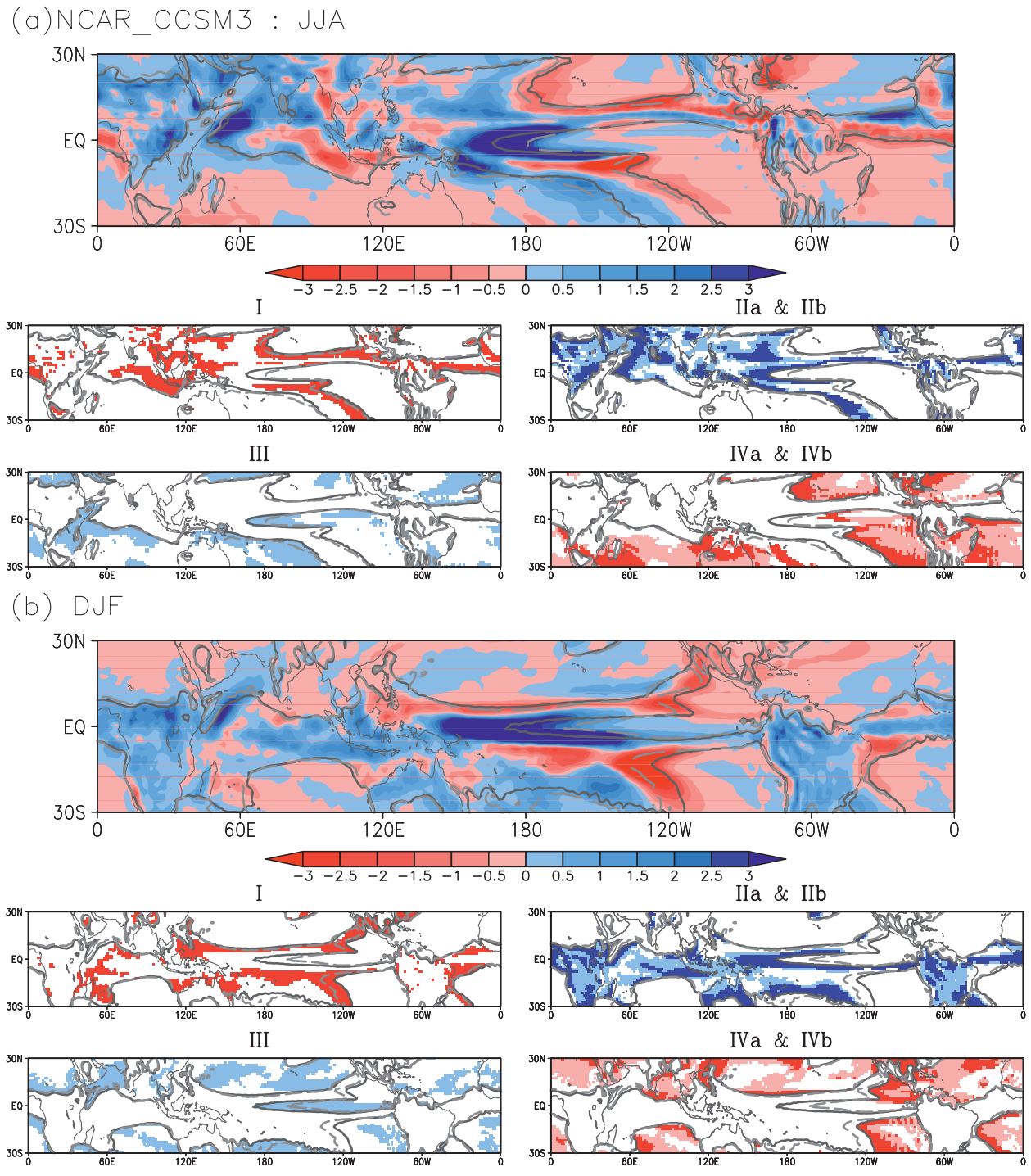

FIG. 2. Summary of 6 subregions, using the NCAR CCSM3 model (as in Figs. 1f,p) as an example: (a) JJA and (b) DJF, which are shaded with precipitation anomalies. Thick solid (dashed) curves denote the boundary of convergence zones (as defined by climatological moisture convergence) in the period of 1961–90 (2070–99). Dark (light) blue shading in subset II is for the area IIa (IIb) and dark (light) red shading in subset IV is for the area Iva (IVb).

term is mainly associated with the nonlinear effect of $-\langle \omega' \partial_P h' \rangle$ since mean upward motion over convective margins is not as large as in convective regions and ω' becomes comparable to $\bar{\omega}$, that is, a shift of convective margins. Other effects, such as enhanced longwave radiation cooling outpaced by increased latent heating, which stabilizes the atmosphere, may also play a role in some specific regions. Overall for the spatial distribution,

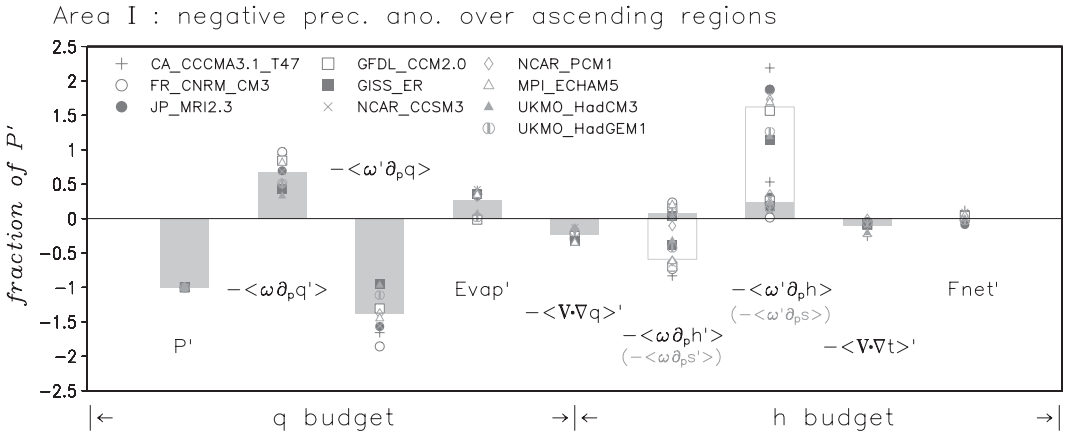

FIG. 3. As in Fig. 1 but for the moisture (1) and moist static energy (3) budget terms (dark shading bars) averaged over the area I, climatologically ascending regions with negative precipitation anomalies ($-\langle\bar{\omega}\partial_p\bar{q}\rangle > 0$ and $P' < 0$; see Table 2), in JJA. Each term is normalized by the precipitation anomalies. The bars are the ensemble mean of 10 CGCMs. The flux-related terms $F^{net'}$ include only 8 models, so no ensemble mean is drawn. The light shading bars, overlapping with $-\langle\omega'\partial_p\bar{h}\rangle$ and $-\langle\bar{\omega}\partial_p h'\rangle$, are $-\langle\omega'\partial_p\bar{s}\rangle$ and $-\langle\bar{\omega}\partial_p s'\rangle$, respectively.

mechanisms for weakening the ascending motion over the area I are much more complicated than the spatial averages indicate, but the upped-ante mechanism still dominates more than half of these areas, such as the South Pacific and South Atlantic convergence zones (Fig. 6).

b. *Positive precipitation anomalies within ascending regions*

Over the ascending regions with positive precipitation anomalies (area II), the moisture and MSE budgets are examined in Fig. 7. The positive precipitation anomalies are around 0.5 mm day^{-1} K^{-1} (Table 3). The dominant term on the right of the moisture budget Eq. (1) is $-\langle\bar{\omega}\partial_p q'\rangle$, which is associated with the direct moisture effect (CN04 terminology) or the thermodynamic component (HS06 terminology). In a warmer climate, the mean circulation transports more moisture vertically because the increased moisture induced by global warming is concentrated in the lower troposphere. The convergence feedback term $-\langle\omega'\partial_p\bar{q}\rangle$ is positive, but its contribution to the positive precipitation anomalies is relatively small. In other words, the dynamic feedback via anomalous vertical motion averaged over these regions is not as important as in the area I shown in Figs. 3 and 5. The evaporation change is positive, while the horizontal moisture advection $-\langle\mathbf{v}\cdot\nabla q\rangle'$ has almost no change in these areas. Compared to the moisture budget averaged over the area I (Fig. 3), the most distinct difference is $-\langle\omega'\partial_p\bar{q}\rangle$: a strong negative contribution to the precipitation change over the area I (Fig. 3) and a weak positive contribution to the precipitation change over the area II (Fig. 7a). Thus, the dynamic feedback to tropical precipitation anomalies is weak when *averaged* over the ascending regions with positive precipitation anomalies (area II), but it is much stronger in the ascending regions with negative precipitation anomalies (area I). We emphasize "averaged" because this does not necessarily hold locally.

Further examining the spatial pattern of $-\langle\omega'\partial_p\bar{q}\rangle$, both positive and negative anomalies are found (Fig. 8), which is very different from the distribution of $-\langle\omega'\partial_p\bar{q}\rangle$ over the area I shown in Fig. 5. Positive $-\langle\omega'\partial_p\bar{q}\rangle$ tends to occur over the areas with stronger positive precipitation anomalies, with magnitude between 0.3 and 0.6 mm day^{-1} K^{-1} in the domain average, while

TABLE 2. Summary of tropical subregions.

Climatological condition	Precipitation anomaly	Vertical velocity anomaly	Subregion
Convergence zones	$P' < 0$	$-\langle\omega'\partial_p\bar{q}\rangle < 0$ (weakening of ascent)	I
	$P' > 0$	$-\langle\omega'\partial_p\bar{q}\rangle > 0$ (strengthening of ascent)	IIa
		$-\langle\omega'\partial_p\bar{q}\rangle < 0$ (weakening of ascent)	IIb
Subsidence regions	$P' > 0$	$-\langle\omega'\partial_p\bar{q}\rangle > 0$ (weakening of descent)	III
	$P' < 0$	$-\langle\omega'\partial_p\bar{q}\rangle < 0$ (strengthening of descent	IVa
		$-\langle\omega'\partial_p\bar{q}\rangle > 0$ (weakening of descent)	IVb

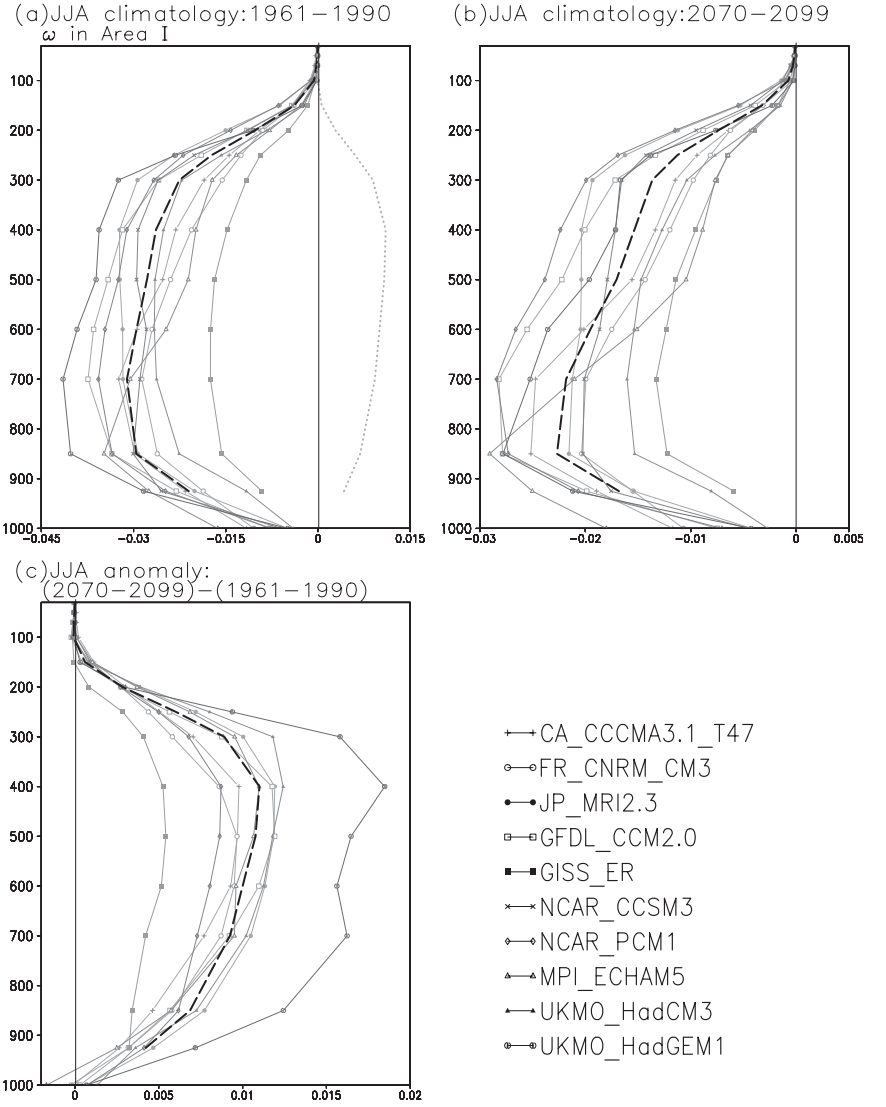

FIG. 4. Vertical profile of (a) mean JJA vertical velocity in 1961–90 ($\bar{\omega}$), (b) mean JJA vertical velocity in 2070–99 ($\bar{\omega}$), and (c) JJA vertical velocity differences for the 2070–99 averages minus the 1961–90 climatology (ω') averaged over the area I (see Table 2). The thick dashed line is the ensemble mean of 10 CGCMs. The dotted line in (a) is the ensemble mean of ω' obtained from (c).

negative $-\langle\omega'\partial_p\bar{q}\rangle$ tends to occur over the boundary of these positive $-\langle\omega'\partial_p\bar{q}\rangle$ areas with precipitation anomalies around 0.1–0.25 mm day^{-1} K^{-1}. Apparently, the small value of $-\langle\omega'\partial_p\bar{q}\rangle$ averaged over the positive precipitation anomaly areas (area II) is due to the cancellation of those positive and negative anomalies. The regions of anomalous descent, yielding negative $-\langle\omega'\partial_p\bar{q}\rangle$ but with positive precipitation anomalies, imply that tropical precipitation can still be enhanced even though the ascending motion over the convective regions is weakened in a warmer climate. Recall from the previous section that the converse does not occur; that is, negative precipitation anomalies are unlikely to be associated with strengthened ascending motion (Fig. 5) since no robust mechanism would allow it.

Because the positive precipitation region has both signs of ω' terms, we examine the budgets for subregions associated with each: one with $-\langle\omega'\partial_p\bar{q}\rangle > 0$ (area IIa), indicating a strengthening of the ascending motion, and the other with $-\langle\omega'\partial_p\bar{q}\rangle < 0$ (area IIb), indicating a weakening of the ascending motion. Over the area IIa, the averaged $-\langle\omega'\partial_p\bar{q}\rangle$ is positive and greater than $-\langle\bar{\omega}\partial_p q'\rangle$, so the convergence feedback $-\langle\omega'\partial_p\bar{q}\rangle$ becomes the dominant effect (Fig. 7b). To understand the dynamic feedback associated with ω' the MSE budget is examined. Here $-\langle\omega'\partial_p\bar{q}\rangle$ is smaller than $-\langle\omega'\partial_p\bar{s}\rangle$, so

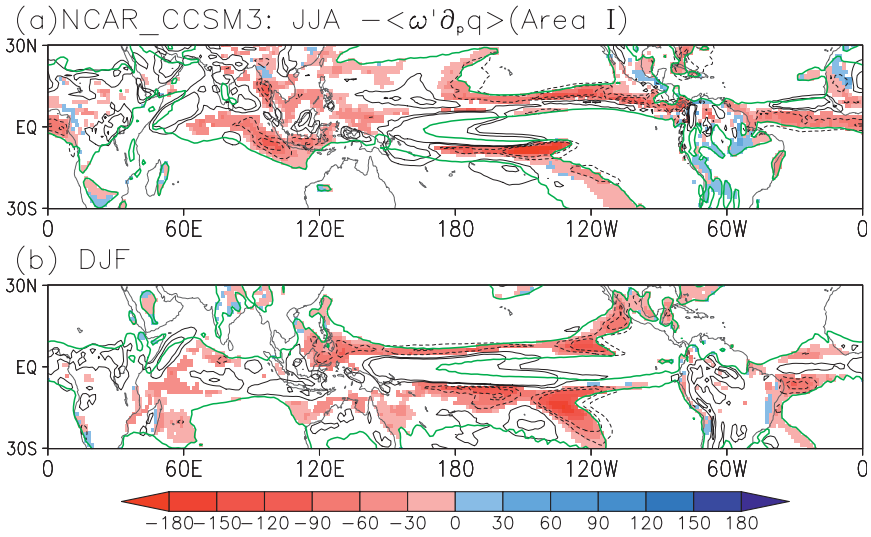

FIG. 5. As in Fig. 1 but for the NCAR CCSM3 $-\langle\omega'\partial_p\bar{q}\rangle$ term (W m^{-2}) over the area I (see Table 2) in (a) JJA and (b) DJF. The contour is the precipitation anomalies and the thick solid line is the $-\langle\bar{\omega}\partial_p\bar{q}\rangle = 0$ contour, which represents the boundary of the convergence zones. The negative values (red shading) indicate anomalous descent: weakening of the ascending motion.

the term on the left of (3) $\langle\omega'\partial_p\bar{h}\rangle$ is positive, which indicates upward vertical motion; that is, $\omega' < 0$. On the right of (3), $-\langle\bar{\omega}\partial_p h'\rangle$, is positive because the amplitude of positive $-\langle\bar{\omega}\partial_p q'\rangle$ is slightly greater than that of negative $-\langle\bar{\omega}\partial_p s'\rangle$. The term $-\langle\bar{\omega}\partial_p h'\rangle$ is associated with the anomalous gross moist stability M', which is negative. In other words, M is reduced, yielding increased ascent and moisture convergence. Other terms, such as horizontal MSE transport $-\langle\mathbf{v}\cdot\nabla(q+T)\rangle'$ and $F^{\text{net}'}$ are both relatively small (not shown). Overall, the anomalous gross moist stability is the dominant factor in this region for inducing positive precipitation anomalies via the dynamic feedback, strengthening the ascending motion, but the direct moisture effect associated with $-\langle\bar{\omega}\partial_p q'\rangle$ in the moisture budget is also important. This can be further explained by (11). The precipitation over convective centers is affected by both M' and M'_q (direct moisture effect) terms.

Over the areas with negative $-\langle\omega'\partial_p\bar{q}\rangle$ (area IIb), the negative contribution of $-\langle\omega'\partial_p\bar{q}\rangle$ opposes positive precipitation anomalies (Fig. 7c). On the other hand, the direct moisture effect $-\langle\bar{\omega}\partial_p q'\rangle$ is positive and its

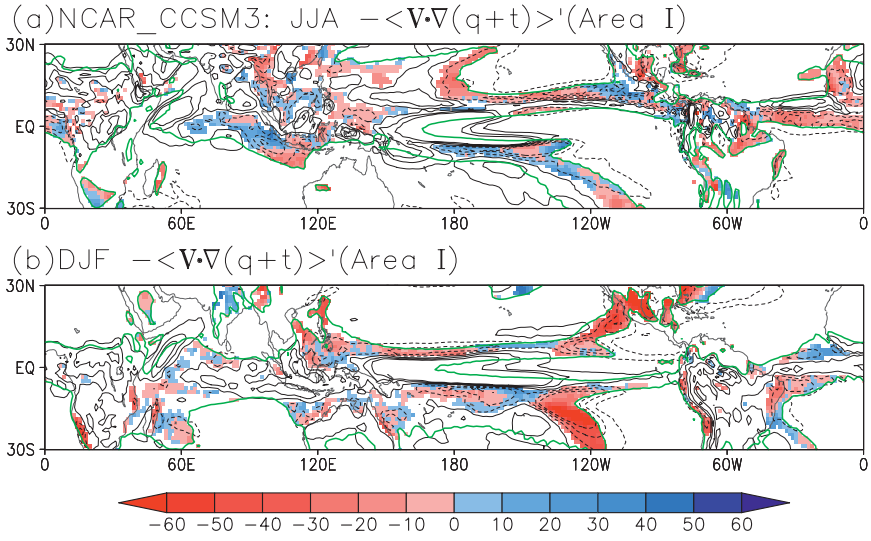

FIG. 6. As in Fig. 5 but for $-\langle\mathbf{v}\cdot\nabla(T+q)\rangle'$ term (W m^{-2}).

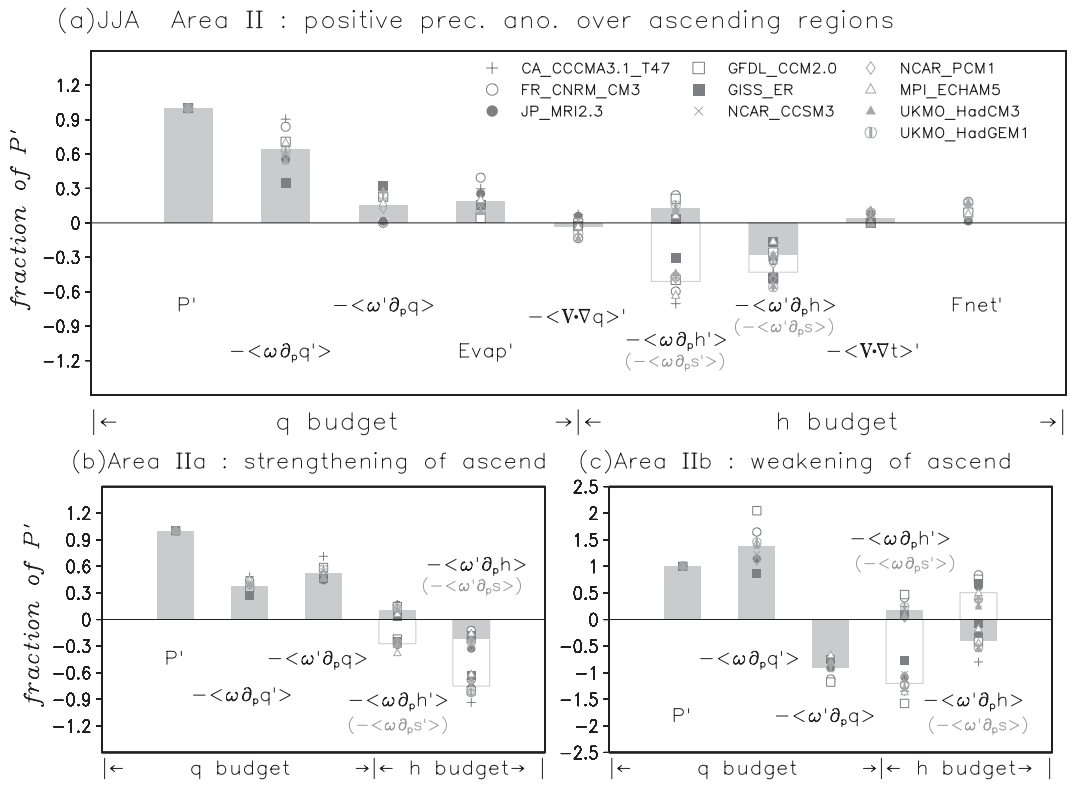

FIG. 7. As in Fig. 3 except for JJA differences averaged over (a) the area II, climatologically ascending regions with positive precipitation anomalies ($-\langle\bar{\omega}\partial_p\bar{q}\rangle > 0$ and $P' > 0$; see Table 2), (b) the area IIa, the area II with anomalous ascent ($-\langle\omega'\partial_p\bar{q}\rangle > 0$), and (c) the area IIb, the area II with anomalous descent ($-\langle\omega'\partial_p\bar{q}\rangle < 0$).

amplitude is much greater than $-\langle\omega'\partial_p\bar{q}\rangle$, inducing positive precipitation anomalies. One might expect that the positive precipitation anomalies induced by positive $-\langle\bar{\omega}\partial_p q'\rangle$ would induce a positive convergence feedback; that is, $\omega' < 0$. However, the ascending motion is actually reduced over these regions. What kind of mechanism weakens the vertical motion over these areas when strong heating associated with convection occurs? The convective heating tends to warm the upper troposphere more than the lower troposphere, so the stability of the atmosphere is increased; that is, $-\langle\bar{\omega}\partial_p s'\rangle < 0$, which tends to reduce the motion. However, this increased stability occurs not only over the area IIb, but also over other convective regions, such as the area IIa. Thus, this should not be a dominant effect for reducing the ascent.

We further examine the vertical profile of mean and anomalous vertical velocities averaged over these areas

TABLE 3. Magnitude of JJA precipitation anomalies (mm day^{-1} K^{-1}) averaged over different subregions for 10 IPCC AR4 models. All the anomalies are normalized by tropically averaged surface temperature anomalies. The values in parentheses are the percentage of each subregion over the entire tropics.

Model	I	IIa	IIb	III	IVa	IVb
CA CCCMA3.1 T 47	−0.17(17)	0.35(13)	0.20(15)	0.10(19)	−0.12(17)	−0.05(19)
FR CNRM CM3	−0.16(19)	0.31(13)	0.13(15)	0.14(31)	−0.11(12)	−0.04(10)
JP MRI2.3	−0.28(22)	0.52(10)	0.22(11)	0.35(20)	−0.15(17)	−0.04(20)
GFDL CCM2.0	−0.26(21)	0.54(10)	0.19(8)	0.14(21)	−0.14(16)	−0.03(24)
GISS-ER	−0.20(20)	0.55(19)	0.18(8)	0.12(16)	−0.14(22)	−0.05(15)
NCAR CCSM3	−0.28(19)	0.53(13)	0.22(12)	0.18(22)	−0.17(15)	−0.04(19)
NCAR PCM1	−0.30(14)	0.47(15)	0.26(11)	0.13(24)	−0.15(17)	−0.04(19)
MPI ECHAM5	−0.22(19)	0.57(13)	0.25(10)	0.16(17)	−0.15(19)	−0.04(22)
UKMO HadCM3	−0.43(19)	0.62(16)	0.22(8)	0.16(15)	−0.18(20)	−0.05(22)
UKMO HadGEM1	−0.49(19)	0.58(14)	0.25(9)	0.18(24)	−0.21(16)	−0.04(18)

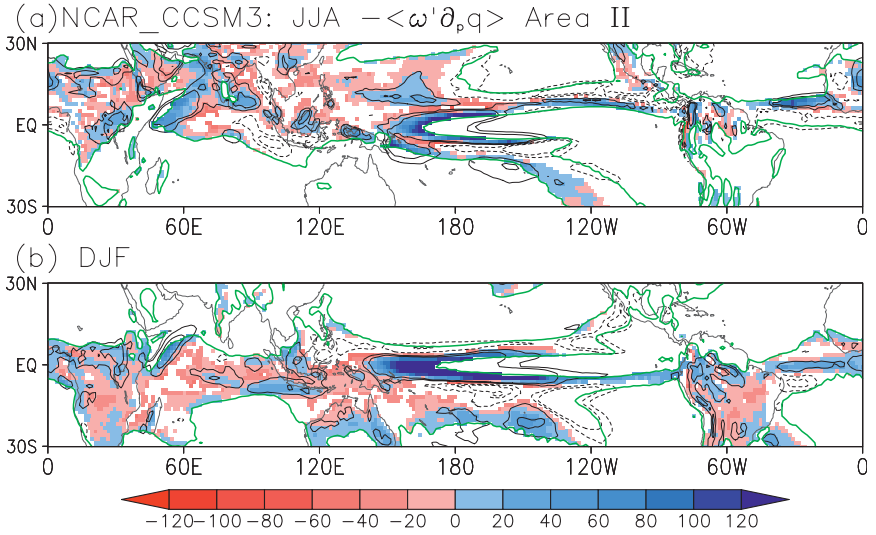

FIG. 8. As in Fig. 5 but for $-\langle\omega'\partial_p\bar{q}\rangle$ term (Wm^{-2}) over the area II (see Table 2).

(Fig. 9). The average profile of the mean vertical velocity is a typical profile of deep convection regions (Fig. 9a). The anomalous vertical velocity (Fig. 9b), on the other hand, has a markedly different vertical profile from the mean vertical velocity (Fig. 9a). Figure 9b shows a weakened ascending motion in the mid- and lower troposphere and strengthened ascending motion in the upper troposphere about 250–100 hPa. This indicates a change of the vertical profile of convection, which tends to slightly increase the depth of the upward vertical velocity. This is consistent with a deepening of convection. Several studies (Holzer and Boer 2001; Santer et al. 2003; International Ad Hoc Detection and Attribution Group 2005) indicate a lifting of tropopause during a warmer climate, which may be related.

We can interpret this in terms of the gross moist stability. According to (10), positive M' can weaken the ascending motion associated with convection. The increased low-level moisture during global warming increases M_q, that is, tends to reduce M. The increased s associated with increased temperature tends to enhance M through M_s. These opposing effects are seen in the opposite signs of $-\langle\bar{\omega}\partial_p q'\rangle$ and $-\langle\bar{\omega}\partial_p s'\rangle$ in both areas IIa and IIb in Fig. 7 (also seen in Fig. 3). If the vertical profile of the vertical velocity changes, it can also change the value of M, such as in the cloud-top effect discussed in Yu et al. (1998). When the depth of convection increases, MSE is redistributed to a deeper column by including higher MSE (or dry static energy) from the upper troposphere, so M is increased, that is, $M' > 0$, and the stability of the atmosphere is enhanced. In Fig. 7c, this contribution is in the $-\langle\omega'\partial_p\bar{h}\rangle$. To better discuss this, consider

$$\langle\omega\partial_p h\rangle' = \langle\bar{\omega}\partial_p h'\rangle + \langle\omega'\partial_p\bar{h}\rangle_{\text{fixed}} + \langle\omega'\partial_p\bar{h}\rangle_{p_T}, \qquad (14)$$

where the first term would correspond to $M'_h\nabla\cdot\bar{\mathbf{v}}_1$, where M'_h represents the anomaly solely due to variations of h, and the second term is due to variations of ω' that can be captured by projecting onto fixed vertical structure, that is, it corresponds to $\bar{M}\nabla\cdot\mathbf{v}'_1$. The third term is associated with changes in vertical structure of ω and, under further assumptions used in Yu et al. (1998), would roughly correspond to $M'_{p_T}\nabla\cdot\bar{\mathbf{v}}_1$, which was due to changes in the depth of convection. The $\langle\omega'\partial_p\bar{s}\rangle$ in our diagnostics can be viewed as having contributions from both $\langle\omega'\partial_p\bar{s}\rangle_{\text{fixed}}$ and $\langle\omega'\partial_p\bar{s}\rangle_{p_T}$. It is the change in vertical structure that is implicated in the reduction of upward vertical velocity in this region.

In most regions, including the area IIa in Fig. 7b, the magnitude of $\langle\omega'\partial_p\bar{s}\rangle$ is larger than $\langle\omega'\partial_p\bar{q}\rangle$, which can be thought of as positive $\bar{M}$ (assuming vertical structure variations are small). In the area IIa, the moistening due to warming in $-\langle\bar{\omega}\partial_p q'\rangle$ yields a reduction in $\bar{M}$ that is only partly compensated by $-\langle\bar{\omega}\partial_p s'\rangle$, causing an increase in vertical velocity, giving a positive feedback. In the area IIb (Fig. 7c), the magnitude of $\langle\omega'\partial_p\bar{s}\rangle$ is instead smaller than $\langle\omega'\partial_p\bar{q}\rangle$ because it includes the effect of the deepened profile increasing the effective moist stability. Turning to the simplified equations, this is analogous to

$$(M\nabla\cdot\mathbf{v}_1)' = \bar{M}\nabla\cdot\mathbf{v}'_1 + M'_h\nabla\cdot\bar{\mathbf{v}}_1 + M'_{p_T}\nabla\cdot\bar{\mathbf{v}}_1, \qquad (15)$$

with $M'_{p_T} > 0$. The M'_q increases with moisture, but the effects of M'_{p_T} (with a contribution from s' in M'_h) more than compensate. Thus, the balance requires negative

$\nabla \cdot \mathbf{v}_1'$, that is, a reduction in ascent. In summary, the weakening of the ascent appears to be tied to the increased depth of the rising motion.

4. Precipitation changes over subsidence regions

a. Positive precipitation anomalies within descending regions

Figure 10 shows both moisture and MSE budgets averaged over the subsidence regions but with positive precipitation anomalies (area III). For the spatial average, the positive precipitation anomalies are around 0.1–0.3 mm day^{-1} K^{-1} (Table 3), which have a similar magnitude to those averaged over the ascending areas with weakened tropical circulation (area IIb), that is, $-\langle\omega'\partial_p\bar{q}\rangle < 0$, but less than those averaged over ascending regions with enhanced tropical circulation (area IIa), that is, $-\langle\omega'\partial_p\bar{q}\rangle > 0$. In the moisture budget, the positive precipitation anomalies are mainly associated with $-\langle\omega'\partial_p\bar{q}\rangle$. The term $-\langle\bar{\omega}\partial_p q'\rangle$ tends to reduce precipitation since the mean descending motion transports relatively dry air from upper troposphere to lower troposphere. Evaporation has a positive contribution to precipitation change, while the horizontal moisture advection $-\langle\mathbf{v}\cdot\nabla q\rangle'$ in the spatial average has little contribution. Overall, $-\langle\omega'\partial_p\bar{q}\rangle$ is the dominant term for balancing positive precipitation anomalies. Positive $-\langle\omega'\partial_p\bar{q}\rangle$ is associated with anomalous ascending motion; that is, the subsidence over these regions is reduced. The anomalous ascent occurs not only in the spatial average, but also over almost every grid point (Fig. 11). In other words, the positive precipitation anomalies over subsidence regions are only associated with anomalous ascending motion.

Furthermore, regions with large values of $-\langle\omega'\partial_p\bar{q}\rangle$ coincide with stronger positive precipitation anomalies in Fig. 11. These areas are close to the boundary of convection zones, implying a shift of the convective margin. Comparing $\bar{\omega}$ and ω' averaged over these regions, the magnitude of ω' is slightly greater than $\bar{\omega}$ (not shown), so these regions do tend to shift from climatological descending areas into ascending areas in a warmer climate. We turn to the MSE budget (Fig. 10) to examine possible processes that induce such upward anomalous motion. Comparing $-\langle\bar{\omega}\partial_P s'\rangle$ and $-\langle\bar{\omega}\partial_p q'\rangle$, we note $-\langle\bar{\omega}\partial_p h'\rangle$ is small, and of the wrong sign to force anomalous ascent (analogous to $-M'\nabla\cdot\bar{\mathbf{v}}_1$ being negative, as expected for $M' < 0$ because of moistening and $\nabla\cdot\bar{\mathbf{v}}_1 < 0$). In the MSE budget, only $F^{\text{net}'}$ and the horizontal temperature transport $-\langle\mathbf{v}\cdot\nabla T\rangle'$ have a positive contribution, implying that these balance the ascent. Each is important in different regions. Examining the spatial distribution of the F_s', a component of $F^{\text{net}'}$, over these regions (not shown), positive F_s' coincides well with the strong positive $-\langle\omega'\partial_p\bar{q}\rangle$, which occurs mostly over the equatorial central Pacific, the areas with strong ocean feedback (Chou et al. 2006), for example, positive heat flux anomalies from ocean to the atmosphere. This strong feedback is usually associated with El Niño–like SST anomalies over the equatorial eastern and central Pacific, which have been discussed by many studies (e.g., Knutson and Manabe 1995; Lorenz and DeWeaver 2007a; Meehl et al. 2007; Meehl and Washington 1996; Teng et al. 2006). Another component of $F^{\text{net}'}$, F_t', which is associated with increased clouds resulting from a dynamic component of cloud changes (Bony et al. 2004) in these regions, is positive. This indicates that positive cloud–radiative feedback via longwave radiation exceeds negative shortwave cloud–radiative feedback and will further enhance the convection over these regions. We also examined the descending areas with weak positive precipitation anomalies, which usually are located at higher latitudes, away from convection zones. Over these regions, $-\langle\omega'\partial_p\bar{q}\rangle$ is much weaker than the descending areas with stronger positive precipitation anomalies. Here F_s' and F_t' are relatively weak, with both positive and negative anomalies throughout the regions. However, a stronger positive $-\langle\mathbf{v}\cdot\nabla T\rangle'$ is found over these areas, possibly because of the change of midlatitude storms in a warmer climate (Lorenz and DeWeaver 2007b).

b. Negative precipitation anomalies within descending regions

Figure 12 shows the moisture budget averaged over the descending areas with negative precipitation anomalies (area IV). Negative precipitation anomalies are mainly associated with negative $-\langle\bar{\omega}\partial_p q'\rangle$. The value of $-\langle\omega'\partial_p\bar{q}\rangle$ is negative and its magnitude is much less than those in the area in shown in Fig. 10. This implies weak anomalous descending motion and a strengthening of the subsidence. Strong positive evaporation anomalies and negative $-\langle\mathbf{v}\cdot\nabla q\rangle'$ are also found. Over these regions, a part of moisture supplied by local evaporation is transported out of these regions, which is a common process in subsidence regions. Overall, the negative precipitation anomalies over these regions is due to the direct moisture effect (HS06's thermodynamic component), that is, $-\langle\bar{\omega}\partial_p q'\rangle$, but with an opposite sign to those in the convergence zones (Fig. 7). Examining the spatial distribution of $-\langle\omega'\partial_p\bar{q}\rangle$ (Fig. 13), positive and negative anomalies coexist, which is very different from the area III, where positive $-\langle\omega'\partial_p\bar{q}\rangle$ dominates. The cancellation of positive and negative $-\langle\omega'\partial_p\bar{q}\rangle$ makes the contribution of the spatially averaged $-\langle\omega'\partial_p\bar{q}\rangle$ secondary in Fig. 12,

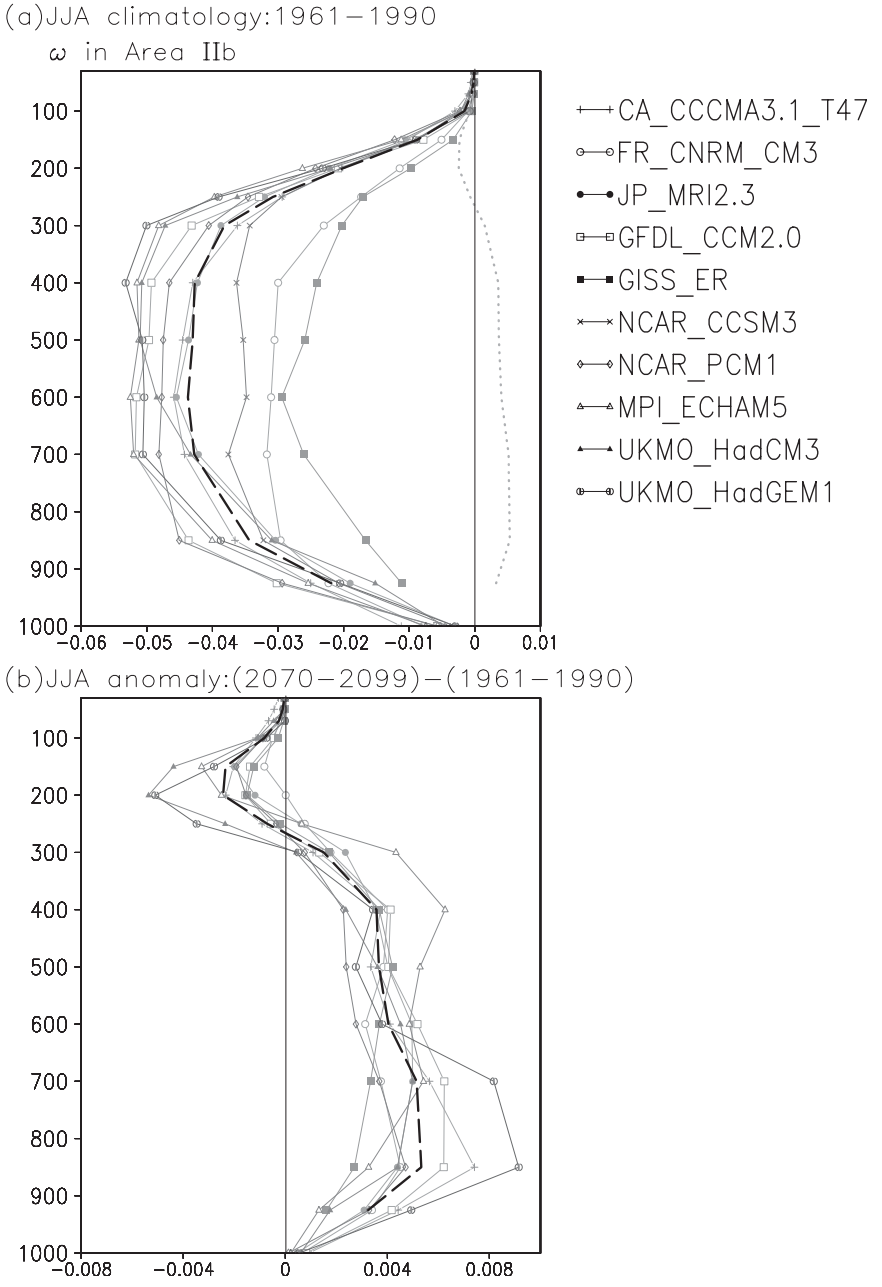

FIG. 9. Vertical profile of (a) mean JJA vertical velocity in 1961–90 ($\bar{\omega}$) and (b) JJA vertical velocity differences for the 2070–99 averages minus the 1961–90 climatology (ω') averaged over the area IIb (see Table 2). The thick dashed line is the ensemble mean of 10 CGCMs. The dotted line in (a) is the ensemble mean of ω' obtained from (b).

consistent with our argument following (9)–(12) that spatial averaging helps justify the HS06 approximation. The negative $-\langle\omega'\partial_p\bar{q}\rangle$ occurs mostly near the boundary of the convergence zones, especially for $-\langle\omega'\partial_p\bar{q}\rangle$ with larger negative magnitudes. These larger negative $-\langle\omega'\partial_p\bar{q}\rangle$ are just next to those ascending areas with the negative precipitation anomalies (area I). The positive $-\langle\omega'\partial_p\bar{q}\rangle$, on the other hand, occur at areas away from convection zones and their amplitudes are relatively smaller than those negative $-\langle\omega'\partial_p\bar{q}\rangle$. Table 3 shows that the magnitude of the negative precipitation anomalies over the area with negative $-\langle\omega'\partial_p\bar{q}\rangle$ (between

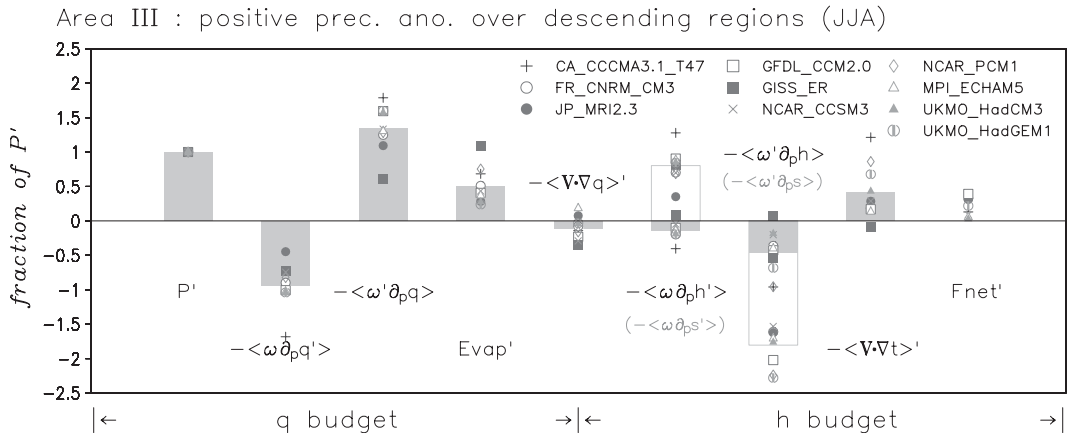

FIG. 10. As in Fig. 3 but for JJA differences averaged over the area III, climatologically descending regions with positive precipitation anomalies ($-\langle\bar{\omega}\partial_p\bar{q}\rangle < 0$ and $P' > 0$; see Table 2).

-0.1 and -0.2 mm day^{-1} K^{-1}) is greater than those over the area with positive $-\langle\omega'\partial_p\bar{q}\rangle$ (between -0.03 and -0.05 mm day^{-1} K^{-1}).

We thus divide the subsidence regions with negative precipitation anomalies into two parts: one with negative $-\langle\omega'\partial_p\bar{q}\rangle$ (area IVa) and the other with positive $-\langle\omega'\partial_p\bar{q}\rangle$ (area IVb). We first discuss the regions with negative $-\langle\omega'\partial_p\bar{q}\rangle$, where subsidence is enhanced since these regions are dominated by descending motion climatologically. In the moisture budget averaged over the area IVa (Fig. 14a), $-\langle\omega'\partial_p\bar{q}\rangle$ becomes a dominant term for contributing to negative precipitation anomalies, while $-\langle\bar{\omega}\partial_p q'\rangle$ becomes secondary. Evaporation is increased, but $-\langle\mathbf{v}\cdot\nabla q\rangle'$ has little change. Even though the area IVa is just next to the ascending regions with negative $-\langle\omega'\partial_p\bar{q}\rangle$ (area I), their moisture and MSE budgets can be very different. Over the climatological descending regions, convection occurs not as often as in convection zones, so the reduced latent heating associated with negative precipitation anomalies, which is strongly compensated by the effect of tropospheric warming, contributes little to the downward anomalous motion. Climatologically speaking, the diabatic heating due to subsidence is usually balanced by longwave radiation cooling. The anomalous outgoing longwave radiation (OLR) is enhanced almost everywhere (not shown) because of less cloudiness and warmer surface and air temperature. The increased longwave

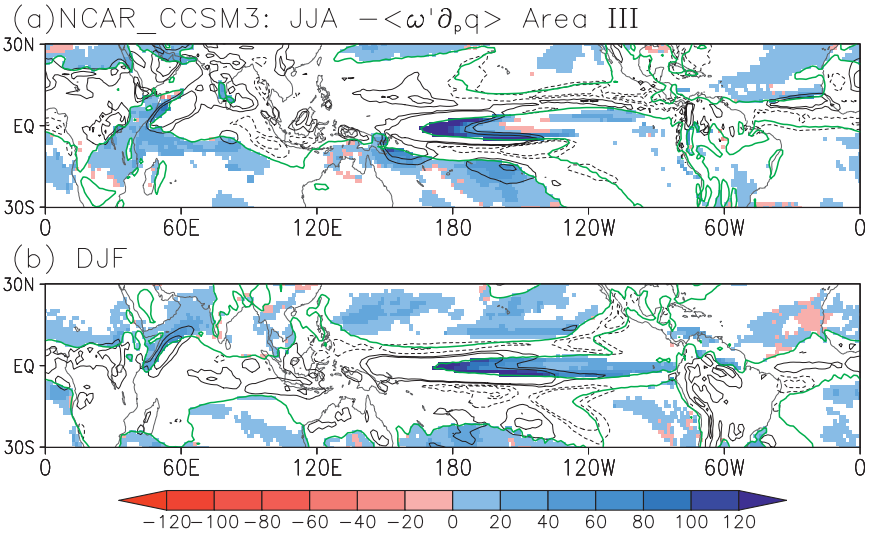

FIG. 11. As in Fig. 5 but for $-\langle\omega'\partial_p\bar{q}\rangle$ term (Wm^{-2}) over the area in (see Table 2). The positive values (blue shading) indicate anomalous ascent: weakening of subsidence.

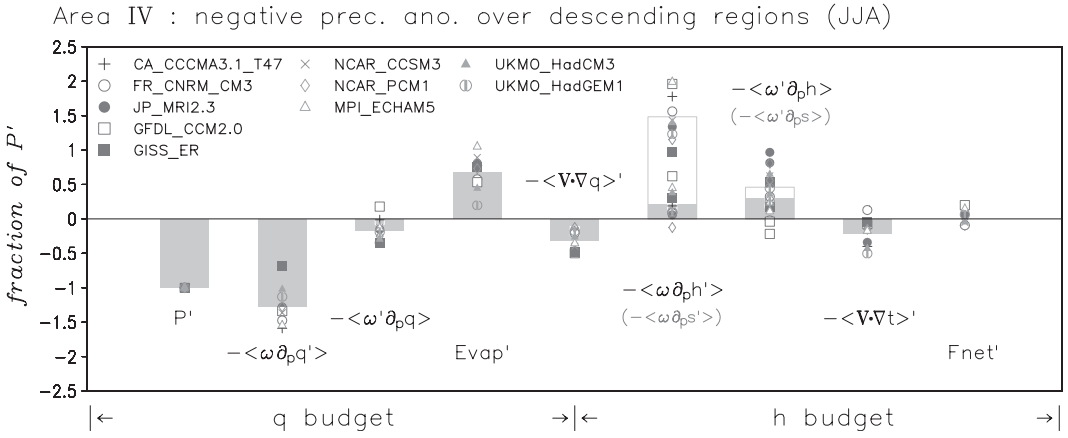

FIG. 12. As in Fig. 3 but for JJA differences averaged over the area IV, climatologically descending regions with negative precipitation anomalies ($-\langle\bar{\omega}\partial_p\bar{q}\rangle < 0$ and $P' < 0$; see Table 2).

cooling can enhance subsidence over the descending regions (Knutson and Manabe 1995). Another interesting point in the MSE budget is the relatively strong negative $-\langle\mathbf{v}\cdot\nabla T\rangle'$. Examining the spatial pattern of $-\langle\mathbf{v}\cdot\nabla T\rangle'$, negative values are found over more than 70% of these areas and their magnitude is relatively large (not shown). This implies that cold advection, which may be associated with the Hadley circulation (Trenberth and Stepaniak 2003), can also be a factor for enhancing the subsidence over the climatological descending regions.

We next examine the regions with positive $-\langle\omega'\partial_p\bar{q}\rangle$ (area IVb), where the descending motion is reduced. Those areas are mostly far away from convection zones and have relatively cold SST beneath, such as the eastern Pacific cold tongue. Over the area IVb, the mean descending motion is usually at maximum with a magnitude of around 0.03 Pa s^{-1} at 500 hPa (Fig. 15). In contrast, the mean descending motion over the area IVa is usually weaker—less than 0.02 Pa s^{-1}. In the moisture budget shown in Fig. 14b, the term $-\langle\bar{\omega}\partial_p q'\rangle$ is negative and larger than the precipitation anomalies; that is, the HS06 thermodynamic component would produce larger P' than actually occurs. The $-\langle\mathbf{v}\cdot\nabla q\rangle'$ term is also negative. Positive evaporation anomalies occur but the main term opposing $-\langle\bar{\omega}\partial_p q'\rangle$ is $-\langle\omega'\partial_p\bar{q}\rangle$ because of anomalous descent.

To understand mechanisms that induce the anomalous ascending motion over the area IVb, we first examine OLR anomalies. Unlike the mostly positive OLR anomalies found over the regions with enhanced subsidence (area IVa), positive and negative OLR

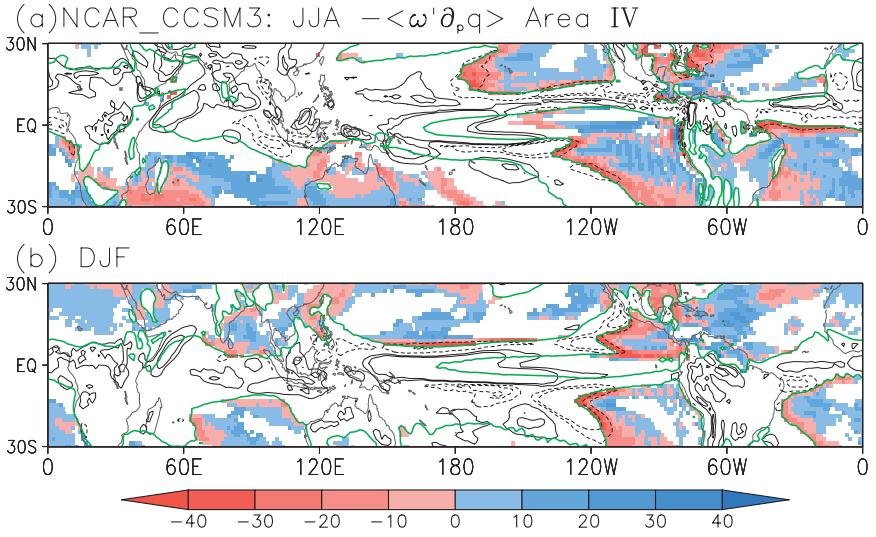

FIG. 13. As in Fig. 5 but for $-\langle\omega'\partial_p\bar{q}\rangle$ over the area IV (see Table 2).

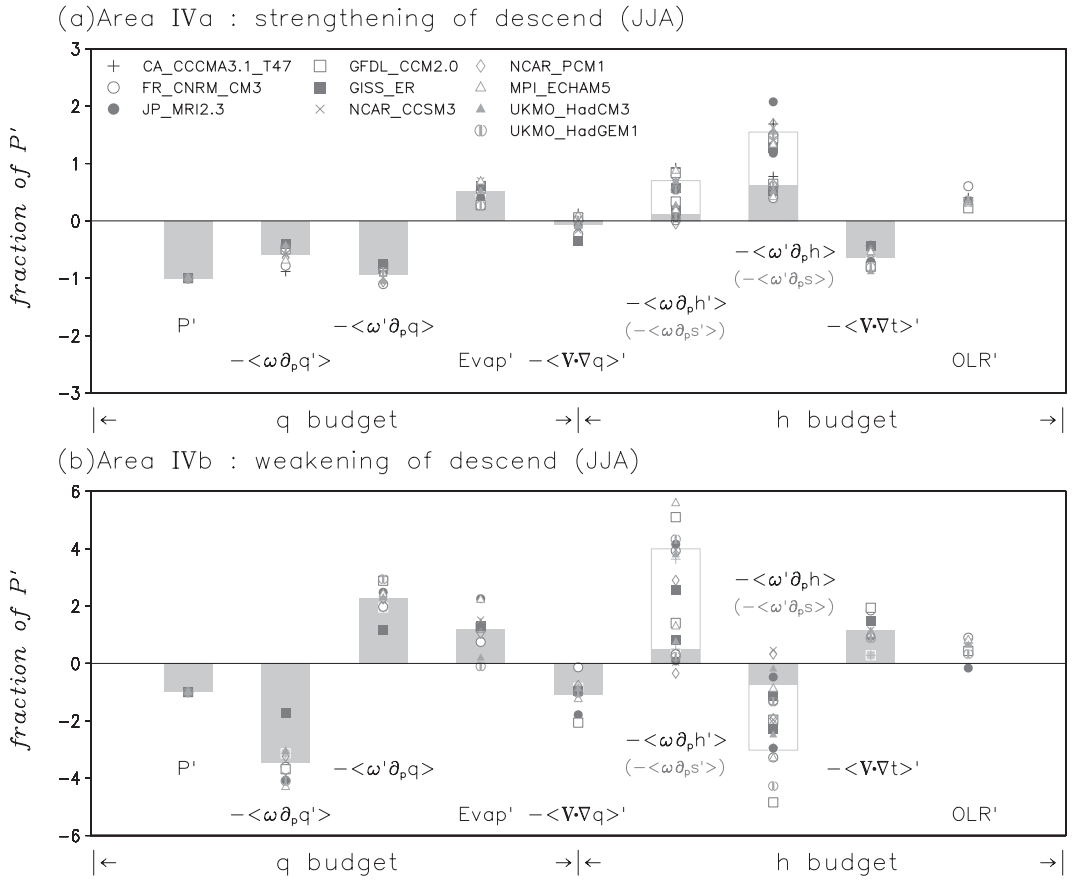

FIG. 14. As in Fig. 3 except for JJA differences averaged over (a) the area IVa, the area IV with anomalous descent $(-\langle\omega'\partial_p\bar{q}\rangle < 0)$, and (b) the area IVb, the area IV with anomalous ascent $(-\langle\omega'\partial_p\bar{q}\rangle > 0)$.

anomalies are equally distributed here. Most negative OLR anomalies are found over oceanic areas where strong upwelling occurs, such as the eastern Pacific. This implies that the atmosphere and oceans are not warm enough to produce positive OLR anomalies consistently over the area IVb. On the other hand, positive $-\langle\mathbf{v}\cdot\nabla T\rangle'$ occupies more than 50% of the area IVb, unlike the negative $-\langle\mathbf{v}\cdot\nabla T\rangle'$ over the area IVa. This implies that positive $-\langle\mathbf{v}\cdot\nabla T\rangle'$ (warm advection) contributes somewhat to the reduced subsidence.

We further examine the vertical profile of mean and anomalous vertical velocity averaged over the area IVb. In Fig. 15, the anomalous vertical velocity is enhanced in the mid- and lower troposphere, but is reduced in the upper troposphere (around 250–100 hPa). This implies a change of the vertical profile of subsidence, similar to its counterpart for the change of the vertical profile of convection over the area IIb shown in Fig. 9. Thus, the associated tropical circulation over both ascending and descending branches is weakened because of the change of the vertical profile of the tropical circulation.

5. Discussion and conclusions

The tropical precipitation change under global warming reveals considerable disagreements among climate models at the regional scale, so attempting to find common features and mechanisms among the models often involves simplification. Here the attempt is made to provide a bridge between the largest-scale, relatively robust aspects and mechanisms that operate at the regional scale. In particular, the effects of dynamic feedbacks associated with changes in circulation appear to be associated with some of the intermodel discrepancy, but also with some of the strongest precipitation anomalies. The focus here is on changes in climatological means. Changes in rainfall characteristics, such as intensity and frequency, are another important aspect, as reviewed in the introduction.

A coordination of the approaches of CN04 and HS06 is outlined for the ''rich-get-richer'' mechanism—the tendency of convergence zones with large climatological precipitation to receive more precipitation and for subsidence regions with low climatological precipitation

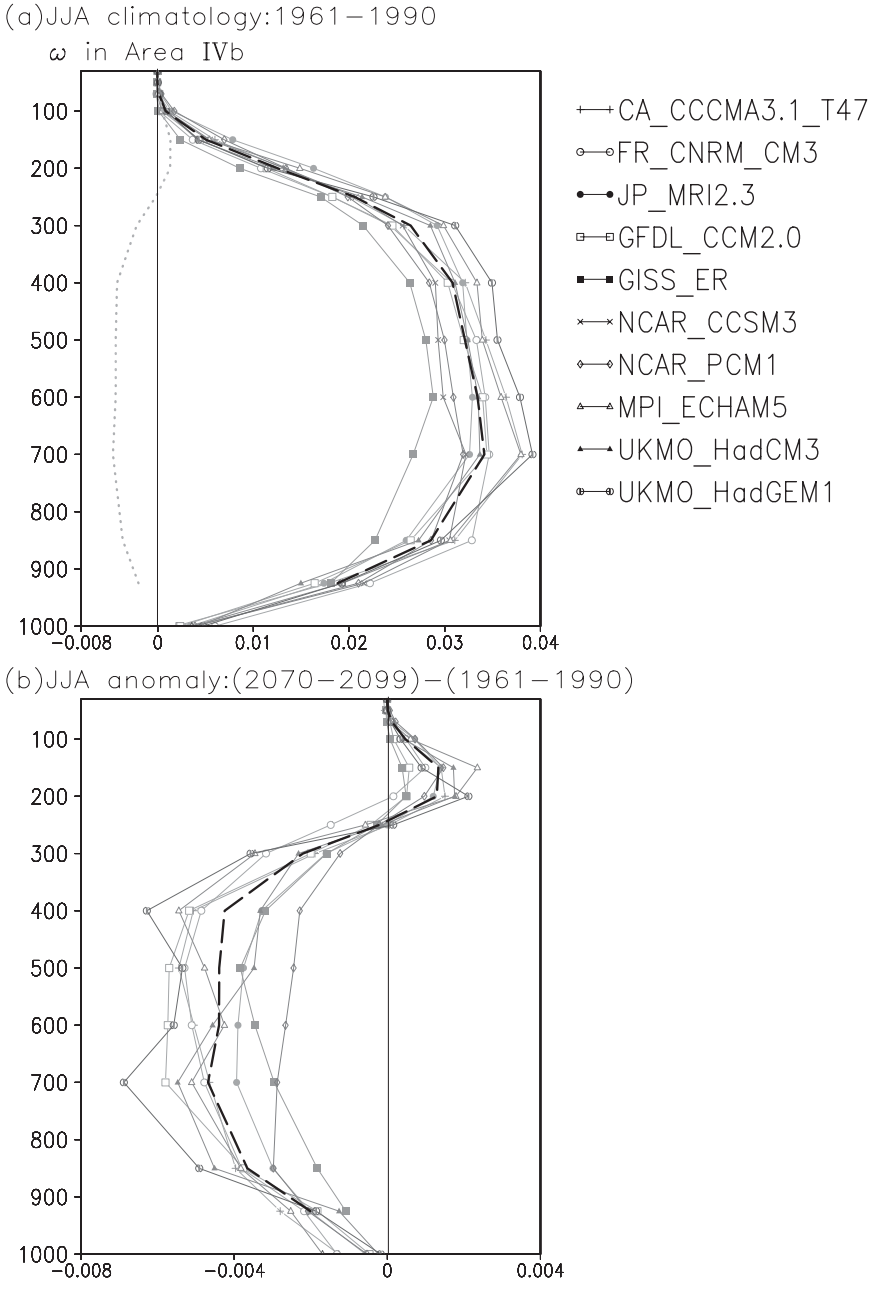

FIG. 15. As in Fig. 9 but for averages of the area IVb (see Table 2).

to experience reductions under global warming. The ''direct moisture effect'' (CN04 terminology) or ''thermodynamic component'' (HS06 terminology) is due to increases in moisture caused by warming acted on by the climatological flow. This is shown to very likely provide a good approximation for precipitation anomalies in spatial averages over an area large enough to reduce convergence anomalies if these occur at scales smaller than the large-scale climatological convergence. HS06 used various forms of averaging (zonal, over convergence zones, ensemble and annual averages) that tend to reduce convergence anomalies in order to bring out the effects of the thermodynamic component and to show a tendency to weakening of the tropical circulation in such averages. CN04 used an approximate formulation of the moist static energy budget to show that changes in the gross moist stability could yield to dynamic feedback on precipitation anomalies because of the thermodynamic component. They postulated that gross moist stability anomalies might differ among models because it is

poorly understood how the gross dry stability component reacts to increases in moisture; because of this, they then proceeded to neglect variations in the dry component.

The large positive and negative precipitation anomalies occurring within the convergence zones (Fig. 1), and associated variations in moisture convergence and other budget anomalies, indicate that averages over the entire convergence zones will miss important effects. To better understand the processes at scales smaller than the convergence zones, moist static energy budgets are examined for subregions within the climatological convergence zones and descent zones defined by moist static energy budget quantities. The climatological ascent/descent regions are subdivided by the sign of the precipitation change. Ascent region positive precipitation anomalies (descent region negative precipitation anomalies) are then further subdivided by vertical velocity anomalies; that is, $\langle \omega' \partial_p \bar{q} \rangle > 0$ or $\langle \omega' \partial_p \bar{q} \rangle < 0$. The tropics are thus divided into six regions (Fig. 2 and Table 2). In each region, the area is large enough to condense information while maintaining consistent properties with respect to ω' and P'. With the caveat that budget terms do not necessarily imply causality, we attempt to interpret these quantities with the aid of the theoretical prototype. Figure 16 summarizes the main effects on tropical precipitation change via dynamic feedbacks for each of the areas discussed below.

a. Convergence zones

In the convergence zones, three major regions are identified: negative precipitation anomalies with weakened tropical circulation, specifically reduced moisture convergence (area I) and positive precipitation anomalies with enhanced (area IIa) and reduced tropical circulation (area IIb).

1) AREA I

The precipitation change is associated with a weakening of the ascending motion, so reduced moisture convergence associated with ω' is the main balance for the precipitation change. Examining mechanisms that induce the descent anomalies, the upped-ante mechanism (Neelin et al. 2003; CN04) associated with dry horizontal advection is a leading effect in most of the regions, while nonlinear effect, such as $-\langle \omega' \partial_p q' \rangle$, which can be associated with a shift of convective margins, and oceanic feedback can also reduce the tropical circulation over some parts of the area I. Changes in sign of the moisture convergence, however, are not a dominant effect here. The importance of dynamic feedback to negative P' is clear, although more than one process can create the weakening of the ascending motion.

2) AREA IIA

The precipitation change is associated with moisture convergence induced by both mean and anomalous vertical velocity, but that which is induced by anomalous vertical velocity is stronger. This is consistent with the convergence feedback contribution to the rich-get-richer mechanism (CN04; Chou et al. 2006): the increased moisture in the lower troposphere destabilizes the atmosphere and increases vertical velocity that is associated with tropical convection.

3) AREA IIB

The increased precipitation is mainly associated with the moisture convergence induced by mean vertical motion, the direct moisture effect or the thermodynamic component, while that which is induced by anomalous vertical velocity actually suppresses tropical precipitation. Examining mechanisms that could induce such weakening of tropical circulation over the area IIb, we found that the change of the vertical profile of convection is responsible. The change of the vertical profile of convection enhances the dry static stability contribution M_s to the gross moist stability M. The increase in M_s is expected to partially compensate increases in low-level moisture (Yu et al. 1998), but in this region the increase actually overcompensates. The increased stability tends to reduce ascending motion. CN04 expressed concern over the lack of theory for M_s variations and then neglected it in intermediate climate model experiments. A second way to derive the HS06 thermodynamic component from CN04 is to assume that M_s' exactly cancels moisture effects in the gross moist stability. Clearly neither of these properly captures the effects occurring in the GCMs. We note that not all convection in the convergence zones changes the vertical profile. The reason for determining where the vertical profile of convection should change is not clear and should be investigated in the future.

b. Subsidence regions

Over the climatological subsidence regions, the tropical precipitation can still be estimated by the moisture budget, but the corresponding tropical circulation could be determined by other processes, such as the balance of the adiabatic warming due to descent and longwave radiation cooling (e.g., Allen and Ingram 2002; Held and Soden 2000; Iwasa et al. 2004). In the subsidence regions, three major areas are also identified: positive precipitation anomalies with upward vertical velocity anomalies (area III) and negative precipitation anomalies with upward (area IVa) and downward (area IVb) vertical velocity anomalies.

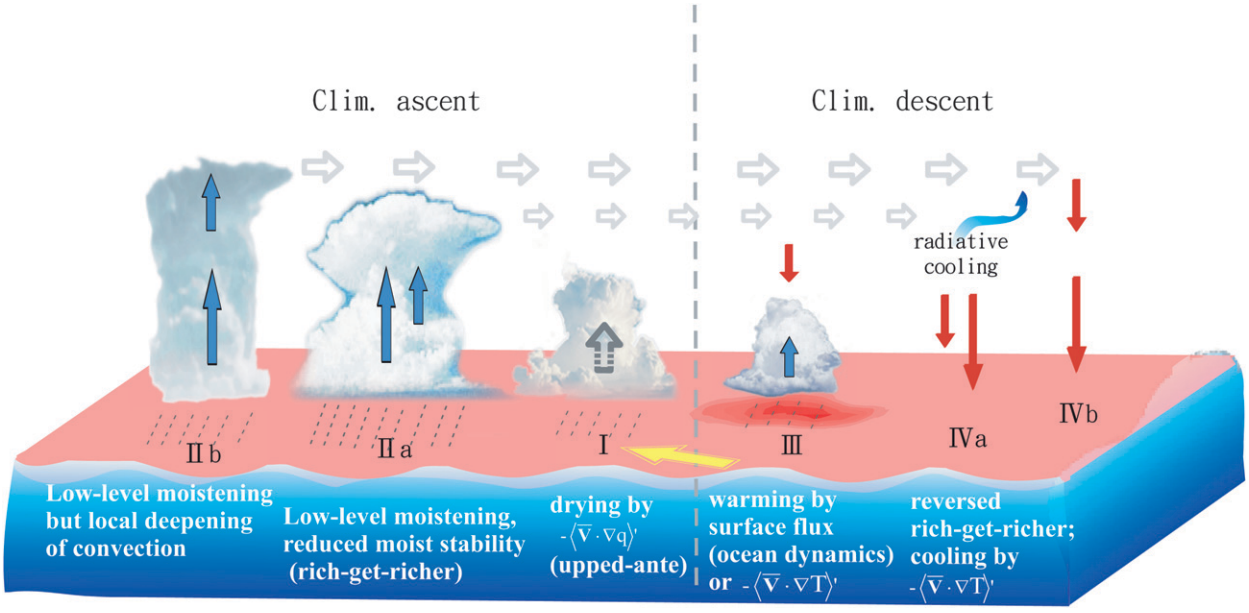

FIG. 16. A schematic diagram summarizing the main mechanisms of tropical precipitation change in 6 subregions. In area II, the rich-get-richer mechanism tends to yield increased precipitation associated with moisture increase in a climatological convergence region; however, in region IIa this is enhanced by convergence feedback associated with reduced moist stability, while in region IIb the increased depth of convection more than compensates moisture effects causing a weakening of the ascent and reducing precipitation anomalies. Region I has negative precipitation anomalies due substantially to the upped-ante mechanism, in which inflow from less-moistened descent regions reduces the fraction of time that the convective threshold is met, thus tending to shift the margin of the convergence zone. Region III descent zone precipitation increases are associated with either surface fluxes supported by ocean dynamics or warm advection. Descent zone precipitation decreases can occur by the rich-get-richer mechanism (with sign reversed) or balances involving cold advection.

1) AREA III

The corresponding subsidence is weakened almost everywhere, so the enhanced precipitation is mainly associated with the vertical moisture transport induced by the anomalous vertical motion. Most of these areas are located just next to convergence zones. While most of the region does not actually switch from moisture divergence to convergence, they are associated with a shift in the margin of the convergence zone between current and future climates. This shift is induced mainly by oceanic feedback via surface heat fluxes, especially in the equatorial cold tongue region. The shift may also be induced by changes of tropical circulation, such as the widening of the Hadley circulation (Lu et al. 2007; Seidel et al. 2007). Over relatively higher latitudes, warm horizontal advection, that is, $-\langle \mathbf{v} \cdot \nabla T \rangle' > 0$, associated with midlatitude storm activity may also play a role for weakening the subsidence.

2) AREA IVA

The corresponding subsidence is enhanced because of stronger longwave radiation cooling, so the precipitation is reduced by the drier downward moisture transport. Some of these regions are located near the convergence zones with negative precipitation anomalies (area I), so the stronger longwave cooling can be associated with either warmer temperature or less cloudiness. The negative horizontal temperature transport, that is, $-\langle \mathbf{v} \cdot \nabla T \rangle' < 0$, also plays a role in enhancing the subsidence.

3) AREA IVB

Enhanced OLR anomalies are not consistently found, so the longwave cooling is not a major contribution. However, the horizontal temperature advection changes signs from the area IVa to the area IVb and becomes positive, so the subsidence over these regions is partially reduced by such warm horizontal advection. Further examination of the vertical profile of the vertical velocity anomalies reveals that the vertical profile of subsidence over these regions is changed, which is consistent with its counterpart of the convergence zones, the change of the vertical profile of convection. In other words, the main mechanism for weakening the downward motion over the subsidence regions is also associated with the change of the vertical profile of tropical circulation.

c. Final remarks

Although at very large scales the direct moisture effect/thermodynamic component can be useful in approximating precipitation changes, the analysis here shows that dynamic feedbacks via changes in vertical velocity are key to the precipitation anomalies of largest magnitude over substantial regions of the tropics in all 10 CGCMs. This applies to anomalies associated with both the upped-ante and rich-get-richer mechanisms. While these dynamical convergence feedbacks can enhance the magnitude of the precipitation anomaly in some regions, regions where they decrease it are surprisingly common. This is shown to be associated with the change of the vertical profile of convection on the dry static energy component of the gross moist stability, M'_s; that is, increased dry static energy transport due to increased depth of convection exceeds the increase in moisture convergence that would accompany M'_q increases. A counterpart occurs in subsidence regions. The fact that this occurs in a spatially inhomogeneous manner underscores the need for better theory for the gross moist stability and presents the additional challenge to the prediction of the strongest precipitation anomalies. Finally, the reduced tropical circulation, averaged over all convergence zones, a robust feature consistently found in climate models (HS06; Vecchi and Soden 2007), is here seen to be mainly due to the combined effect of the upped-ante mechanism and the convection-deepening effect, on a regional basis.

Acknowledgments. This work was supported under National Science Council Grant 96-2628-M-001-019 and National Science Foundation Grant ATM-0645200 (JDN). We acknowledge the modeling groups for providing their data, PCMDI at Lawrence Livermore National Laboratories for collecting the model data, the JSC/CLIVAR Working Group on Coupled Modelling (WGCM) for organizing the model analysis activity, and the IPCC WG1 TSU for technical support. The IPCC Data Archive at Lawrence Livermore National Laboratory is supported by the Office of Science, U.S. Department of Energy.

REFERENCES

Allan, R. P., and B. J. Soden, 2007: Large discrepancy between observed and simulated precipitation trends in the ascending and descending branches of the tropical circulation. *Geophys. Res. Lett.,* **34,** L18705, doi:10.1029/2007GL031460.

——, and ——, 2008: Atmospheric warming and the amplification of precipitation extremes. *Science,* **321,** 1481–1484.

Allen, M. R., and W. J. Gram, 2002: Constraints on future changes in climate and the hydrologic cycle. *Nature,* **419,** 224–232.

Barnett, D. N., S. J. Brown, J. M. Murphy, D. M. H. Sexton, and M. J. Webb, 2006: Quantifying uncertainty in changes in extreme event frequency in response to doubled CO_2 using a large ensemble of GCM simulations. *Climate Dyn.,* **26,** 489–511.

Bony, S., J.-L. Dufresne, H. Le Treut, J.-J. Morcrette, and C. Senior, 2004: On dynamic and thermodynamic components of cloud changes. *Climate Dyn.,* **22,** 71–86.

——, and Coauthors, 2006: How well do we understand and evaluate climate change feedback processes? *J. Climate,* **19,** 3445–3482.

Chou, C., and J. D. Neelin, 2004: Mechanisms of global warming impacts on regional tropical precipitation. *J. Climate,* **17,** 2688–2701.

——, ——, J.-Y. Tu, and C.-T. Chen, 2006: Regional tropical precipitation change mechanisms in ECHAM4/OPYC3 under global warming. *J. Climate,* **19,** 4207–4223.

——, J.-Y. Tu, and P.-H. Tan, 2007: Asymmetry of tropical precipitation change under global warming. *Geophys. Res. Lett.,* **34,** L17708, doi:10.1029/2007GL030327.

Christensen, J. H., and Coauthors, 2007: Regional climate projections. *Climate Change 2007: The Physical Science Basis,* S. Solomon et al., Eds., Cambridge University Press, 847–940.

Chung, C. E., and V. Ramanathan, 2007: Relationship between trends in land precipitation and tropical SST gradient. *Geophys. Res. Lett.,* **34,** L16809, doi:10.1029/2007GL030491.

Cubasch, U., and Coauthors, 2001: Projections of future climate change. *Climate Change 2001: The Scientific Basis,* J. T. Houghton et al., Eds., Cambridge University Press, 525–582.

Dai, A., 2006: Precipitation characteristics in eighteen coupled climate models. *J. Climate,* **19,** 4606–4630.

——, and K. E. Trenberth, 2004: The diurnal cycle and its depiction in the Community Climate System Model. *J. Climate,* **17,** 930–951.

Emori, S., and S. J. Brown, 2005: Dynamic and thermodynamic changes in mean and extreme precipitation under changed climate. *Geophys. Res. Lett.,* **32,** L17706, doi:10.1029/2005GL023272.

Held, I. M., and B. J. Soden, 2000: Water vapor feedback and global warming. *Annu. Rev. Energy Environ.,* **25,** 441–475.

——, and ——, 2006: Robust responses of the hydrological cycle to global warming. *J. Climate,* **19,** 5686–5699.

Holloway, C. E., and J. D. Neelin, 2007: The convective cold top and quasi equilibrium. *J. Atmos. Sci.,* **64,** 1467–1487.

Holzer, M., and G. J. Boer, 2001: Simulated changes in atmospheric transport climate. *J. Climate,* **14,** 4398–4420.

International Ad Hoc Detection and Attribution Group, 2005: Detecting and attributing external influences on the climate system: A review of recent advances. *J. Climate,* **18,** 1291–1314.

Iwasa, Y., Y. Abe, and H. Tanaka, 2004: Global warming of the atmosphere in radiative–convective equilibrium. *J. Atmos. Sci.,* **61,** 1894–1910.

Kharin, V. V., and F. W. Zwiers, 2005: Estimating extremes in transient climate change simulations. *J. Climate,* **18,** 1156–1173.

Knutson, T. R., and S. Manabe, 1995: Time-mean response over the tropical Pacific to increase CO_2 in a coupled ocean–atmosphere model. *J. Climate,* **8,** 2181–2199.

Li, W., R. E. Dickinson, R. Fu, G.-Y. Niu, Z.-L. Yang, and J. G. Canadell, 2007: Future precipitation changes and their implications for tropical peatlands. *Geophys. Res. Lett.,* **34,** L01403, doi:10.1029/2006GL028364.

Lorenz, D. J., and E. T. DeWeaver, 2007a: Tropopause height and zonal wind response to global warming in the IPCC scenario

integrations. *J. Geophys. Res.,* **112,** D10119, doi:10.1029/2006JD008087.

——, and ——, 2007b: The response of the extratropical hydrological cycle to global warming. *J. Climate,* **20,** 3470–3484.

Lu, J., G. A. Vecchi, and T. Reichler, 2007: Expansion of the Hadley cell under global warming. *Geophys. Res. Lett.,* **34,** L06805, doi:10.1029/2006GL028443.

Manabe, S., and R. T. Wetherald, 1975: The effect of doubling CO_2 concentration on the climate of the general circulation model. *J. Atmos. Sci.,* **32,** 3–15.

Meehl, G. A., and W. M. Washington, 1996: El Niño-like climate change in a model with increased atmospheric CO_2 concentrations. *Nature,* **382,** 56–60.

——, J. M. Arblaster, and C. Tebaldi, 2005: Understanding future patterns of increased precipitation intensity in climate model simulations. *Geophys. Res. Lett.,* **32,** L18719, doi:10.1029/2005GL023680.

——, and Coauthors, 2007: Global climate projections. *Climate Change 2007: The Physical Science Basis,* S. Solomon et al., Eds., Cambridge University Press, 747–845.

Milly, P. C. D., K. A. Dunne, and A. V. Vecchia, 2005: Global pattern of trends in streamflow and water availability in a changing climate. *Nature,* **438,** 347–350.

Neelin, J. D., and J.-Y. Yu, 1994: Modes of tropical variability under convective adjustment and the Madden–Julian oscillation. Part I: Analytical theory. *J. Atmos. Sci.,* **51,** 1876–1894.

——, C. Chou, and H. Su, 2003: Tropical drought regions in global warming and El Niño teleconnections. *Geophys. Res. Lett.,* **30,** 2275, doi:10.1029/2003GL018625.

——, M. Münnich, H. Su, J. E. Meyerson, and C. E. Holloway, 2006: Tropical drying trends in global warming models and observations. *Proc. Natl. Acad. Sci. USA,* **103,** 6110–6115.

Rowell, D. P., and R. G. Jones, 2006: Causes and uncertainty of future summer drying over Europe. *Climate Dyn.,* **27,** 281–299.

Santer, B. D., and Coauthors, 2003: Contributions of anthropogenic and natural forcing to recent tropopause height changes. *Science,* **301,** 479–483.

Seager, R., and Coauthors, 2007: Model projections of an imminent transition to a more arid climate in southwestern North America. *Science,* **316,** 1181–1184.

Seidel, D. J., Q. Fu, W. J. Randel, and T. J. Reichler, 2007: Widening of the tropical belt in a changing climate. *Nat. Geosci.,* **1,** 21–24, doi:10.1038/ngeo.2007.38.

Soden, B. J., D. L. Jackson, V. Ramaswamy, M. D. Schwarzkopf, and X. Huang, 2005: The radiative signature of upper tropospheric moistening. *Science,* **310,** 841–844.

Stott, P. A., and J. A. Kettleborough, 2002: Origins and estimates of uncertainty in predictions of twenty-first century temperature rise. *Nature,* **416,** 723–726.

Sun, Y., S. Solomon, A. Dai, and R. W. Portmann, 2007: How often will it rain? *J. Climate,* **20,** 4801–4818.

Teng, H., L. E. Buja, and G. A. Meehl, 2006: Twenty-first-century climate change commitment from a multi-model ensemble. *Geophys. Res. Lett.,* **33,** L07706, doi:10.1029/2005GL024766.

Trenberth, K. E., and D. P. Stepaniak, 2003: Seamless poleward atmospheric energy transports and implications for the Hadley circulation. *J. Climate,* **16,** 3706–3722.

——, and A. Dai, 2007: Effects of Mount Pinatubo volcanic eruption on the hydrological cycle as an analog of geoengineering. *Geophys. Res. Lett.,* **34,** L15702, doi:10.1029/2007GL030524.

——, ——, R. M. Rasmussen, and D. B. Parsons, 2003: The changing character of precipitation. *Bull. Amer. Meteor. Soc.,* **84,** 1205–1217.

——, and Coauthors, 2007: Observations: Surface and atmospheric climate change. *Climate Change 2007: The Physical Science Basis,* S. Solomon et al., Eds., Cambridge University Press, 235–336.

Vecchi, G. A., and B. J. Soden, 2007: Global warming and the weakening of the tropical circulation. *J. Climate,* **20,** 4316–4340.

——, ——, A. T. Wittenberg, I. M. Held, A. Leetmaa, and M. J. Harrison, 2006: Weakening of tropical Pacific atmospheric circulation due to anthropogenic forcing. *Nature,* **441,** 73–76.

Wentz, F. J., L. Ricciardulli, K. Hilburn, and C. Mears, 2007: How much more rain will global warming bring? *Science,* **317,** 233–235.

Wetherald, R. T., and S. Manabe, 2002: Simulation of hydrologic changes associated with global warming. *J. Geophys. Res.,* **107,** 4379, doi:10.1029/2001JD001195.

Wilby, R. L., and T. M. L. Wigley, 2002: Future changes in the distribution of daily precipitation totals across North America. *Geophys. Res. Lett.,* **29,** 1135, doi:10.1029/2001GL013048.

Wilcox, E. M., and L. J. Donner, 2007: The frequency of extreme rain events in satellite rain-rate estimates and an atmospheric general circulation model. *J. Climate,* **20,** 53–69.

Yu, J.-Y., C. Chou, and J. D. Neelin, 1998: Estimating the gross moist stability of the tropical atmosphere. *J. Atmos. Sci.,* **55,** 1354–1372.

Zhang, X., F. W. Zwiers, G. C. Hegerl, F. H. Lambert, N. P. Gillett, S. Solomon, P. A. Stott, and T. Nozawa, 2007: Detection of human influence on twentieth-century precipitation trends. *Nature,* **448,** 461–465.